Open access • Journal Article • DOI:10.1039/C7TB02527K

Recent progress in upconversion luminescence nanomaterials for biomedical applications — Source link

Chengchen Duan, Liuen Liang, Li Li, Run Zhang ...+1 more authors

Institutions: University of Queensland, Macquarie University

Published on: 03 Jan 2018 - Journal of Materials Chemistry B (The Royal Society of Chemistry)

Topics: Photon upconversion

Recent Progresses of Upconversion Luminescence Nanomaterials for Biomedical Applications

Chengchen Duan,[a, †] Liuen Liang,[b, †] Li Li,[a] Run Zhang,[a, *] Zhi Ping Xu[a, *]

[a] Australian Institute for Bioengineering and Nanotechnology, The University of Queensland, St Lucia, QLD, 4072, Australia

[b] ARC Centre of Excellence for Nanoscale BioPhotonics, Department of Physics and Astronomy, Macquarie University, Sydney, NSW, 2109, Australia

Correspondence should be addressed to:

Dr Run Zhang, Email: r.zhang@uq.edu.au

Prof Zhi Ping Xu, Email: z.xu1@uq.edu.au

[†] Equal Contribution to this Review

Abstract

Upconversion nanoparticles (UCNPs) are one kind of luminescence nanomaterials that convert low energy photons to high energy emissions. These nanomaterials have recently attracted enormous attention due to their unique photophysical properties, such as resistance to photobleaching and photoblinking, low background autofluorescence, and long luminescence lifetime. Owing to these unique advantages, UCNPs have been widely examined for biomedical applications, including biosensing, imaging, and theranostics. In this review, we have first summarized the mechanisms for three generally accepted upconversion luminescence processes, *i.e.* lanthanide (Ln) doped upconversion luminescence, dye-sensitized upconversion, and triplet-triplet annihilation upconversion, and then discussed recent advancements on the preparation, functionalization and biomedical applications of each type of UCNPs. The review article is finally concluded with our perspectives on UCNPs' emerging and potential biomedical applications in the near future.

Keywords:

Upconversion nanoparticles; Upconversion luminescence; Imaging and diagnosis; Biosensors; Photodynamic therapy

1. Introduction

Rapid development in design and preparation of the next generation of nano-biomaterials and efforts on exploiting their applications in life science provides new opportunities for the cutting edge chemistry, biology, and biomedical researches. For biomedical applications, the nanomaterials that can visualize the evolution of biological processes and image the interactions between nanomaterials and biomolecules at the cellular or subcellular level are highly aspired. These nanomaterials are normally developed with unique properties for optical, magnetic, acoustic and radiative applications.[1-5] Among them, engineering of optical nanoparticles is emerging as a versatile tool in biomedical applications such as bioanalytical science, biomedical imaging, and imaging guided therapy.[1, 6] These biomedical applications are currently well recognized for their effectiveness in living systems.

Recently, a variety of optical luminescence nanomaterials with excellent sensitivity and high spatial resolution have been developed,[7, 8] such as organic polymers, dendrimers,[9, 10] inorganic quantum dots,[11, 12] noble metal nanoclusters,[13] luminescent dye-doped silica nanoparticles,[8, 14] and lanthanide-doped nanophosphors.[8, 15, 16] Generally, these luminescence nanoparticles feature specific absorption and emission properties that can be functionalized for probing biomolecules inside the cells or tissues. Thus, they have been applied in bio-imaging, biosensing, and imaging guided disease treatment, such as drug/gene delivery and phototherapies.[17-19] In addition, conjugation of specific targeting ligands onto the surface of luminescent nanoparticles, *e.g.* peptides, antibodies and small molecules, allows these nanoparticles as the probes to detect and target the specific cells of interest with high sensitivity and selectivity. More importantly, the therapeutic drugs and genes, such as doxorubicin, RNA, DNA, and photosensitizers, can also be loaded within these luminescent nanoparticles for effective tumor therapies with optical imaging guidance.[20-22]

The luminescence nanomaterials are typically excited by higher energy photons and emitted as lower energy photons, *i.e.,* the emitted light has a longer wavelength, and therefore lower energy, than the excitation photon (down conversion luminescence).[15] Since the late 1990s, anti-Stokes luminescence nanoparticles, namely upconversion nanoparticles (UCNPs), have been reported as a kind of new photoluminescent nanomaterials.[15, 23] In contrast with traditional Stokes photoluminescence (down

conversion luminescence), UCNPs can be photo-excited by deep-penetrating near-infrared (NIR) light and emit ultraviolet (UV), visible or near-infrared radiation via the photon energy upconversion process.[24, 25] This photon conversion process can be performed under a low power light excitation, such as continuous-wave (CW) lasers, and the emission with higher energy can be recorded by a generally used luminescence spectrometers or microscopes.[26, 27] It is noted that the upconversion luminescence is different with two-photon absorption-based luminescence materials, which requires the photon absorption nearly at the same time. Therefore, coherent photon excitation by a high power femtosecond laser (~10^6 W/cm^2) is needed for the two-photon luminescence materials.[12] In addition, investigations on the two-photon absorption process mainly focused on the molecular luminescence materials, which will not be included in this review.

Owing to their unique photon conversion properties, UCNPs have shown great potentials in biomedical applications *in vivo*, in particular in deep tissues. The use of NIR light to elicit photoluminescence in UCNPs enables deeper penetration (measured in centimetres) in biological tissues, which also excites considerably less autofluorescence and exerts less phototoxicity compared to UV and visible light. In addition, UCNPs can serve as a powerful converter to transform NIR irradiation into UV or visible lights that initiates the deep-tissue treatment from photo-responsive therapeutic systems, which cannot be achieved by using UV/Vis excitation agents. At present, lanthanide (Ln) doped upconversion nanocrystals, dye-sensitized upconversion nanoparticles, and triplet-triplet annihilation (TTA)-based UCNPs,[23, 28-30] are being widely investigated to explore their potential biomedical applications in diagnosis, biosensing, imaging and treatment of diseases, such as cancers. This review will firstly summarize the excitation and emission mechanisms based on three upconversion processes, followed by the summary of the development of UCNPs in controlled preparation, surface chemistry, and biomedical applications. The challenging and future perspectives of these luminescent nanomaterials in biomedical applications will be provided as a conclusion.

2. Luminescence mechanisms of upconversion nanomaterials

Upconversion nanomaterials including Ln-doped inorganic nanocrystals and TTA-based UCNPs have undergone rapid development in the past decades. Different with the generally accepted two-photon absorption luminescence, in which the luminescent materials are excited by two photons simultaneously to a virtual state, UCNPs are activated in a step-wise process, where real excitation energy states exist with the components of each nanoparticle. In following sections, the energy transfer mechanisms are briefly presented for Ln-doped, dye-sensitized and TTA UCNPs, respectively.

2.1. Ln-doped UCNPs

Abundant energy states of Ln^{3+} ions endow the Ln-doped nanoparticles enormous opportunities for the energy transfer upconversion processes. These processes are very complicated and can be simply summarized as the excited-state absorption (ESA), energy transfer upconversion (ETU), cooperative sensitization upconversion (CSU), photon avalanche (PA), and energy migration upconversion (EMU),[31, 32] as illustrated in Fig. 1.

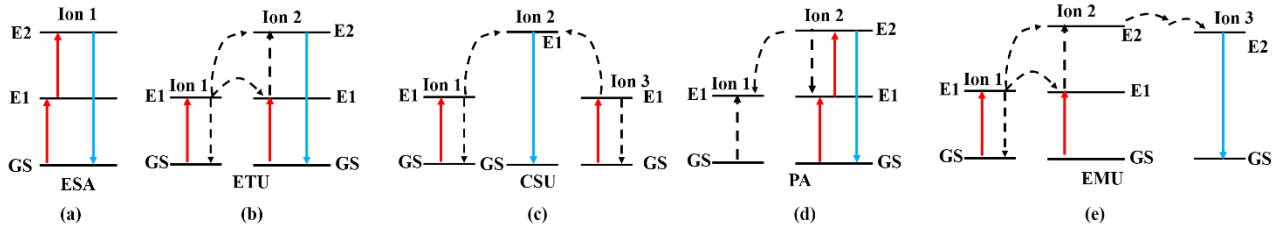

Fig. 1. Upconversion processes for Ln-doped UCNPs. GS: ground state; E1 and E2: excited states; ESA: excited-state absorption; ETU: energy transfer upconversion; CSU: cooperative sensitization upconversion; PA: photon avalanche; EMU: energy migration upconversion.

In ESA, the excitation state or emission state (E2) is formed by absorption two sequential photons through a single ground state (GS) Ln^{3+} ion with appropriate excitation states. As shown in Fig. 1a,

when the GS Ln^{3+} is irradiated by a suitable excitation energy, an intermediate state (E1) is formed, and this E1 state is then excited by a second photon to the E2 state for upconversion emission.[33] Therefore, the emission efficiency is dependent on the stability of the E1 state. Up to date, only limited Ln^{3+} ions, such as Er^{3+}, Ho^{3+}, Tm^{3+}, and Nd^{3+}, are suitable for this mechanism since their excitation states are well matched with the excitation energy of commercial lasers (975 and 808 nm). Although the emission efficiency of ESA upconversion luminescence is independent of doping concentration, the Ln^{3+} doping concentration is normally lower than 1% considering the cross-relaxation of the excitation states.[32]

In the ETU process, two kinds of Ln^{3+} ions, a sensitizer and an activator, are involved in upconversion luminescence (Fig. 1b). Upon irradiation with a suitable laser, both sensitizer and activator are excited to the E1 excitation state by absorbing photons,[34, 35] Then, the sensitizer at the E1 state will transfer its energy to the E1 state of the activator, resulting in the activator excited to the E2 state for upconversion emission. The upconversion emission efficiency is doping concentration dependent (distance between sensitizer and activator) and is normally higher than the ESA process. Similar to ETU, CSU involves two sensitizers and one activator in the upconversion energy transfer (Fig. 1c). The activator here is promoted to its E2 excitation state through energy transfer from two sensitizers at the E1 excitation state. The relaxation of the activator from the E2 state to GS leads to emitting upconversion photons.

PA-based upconversion process is normally much less efficient than ETU. In such an upconversion process, all Ln-dopants are excited with the energy unmatched pump photons, normally higher than the energy gap between the intermediate excitation state and GS.[31] ESA and cross-relaxation may occur until energy population to an intermediate state, and then the E2 energy state of Ln^{3+} ions, producing upconversion luminescence. High pump intensity and long irradiation time are necessary for this upconversion process.

Different from the processes described above, EMU is normally observed from the core-shell Ln-doped UCNP nanomaterials,[36, 37] where the active shell may lead to higher emission efficiency. This upconversion process is firstly reported by Liu's group.[36] In this phenomenon, four kinds of luminescence components, namely a sensitizer, an accumulator, a migrator and an activator with a

suitable concentration, are integrated within one nanoparticle at separate layers. Upon the laser irradiation, the EMU process occurs at the core of the nanoparticle, followed by the step-by-step energy transfer from the accumulator to the activator, producing upconversion luminescence.

Each specific Ln-doped nanoparticle has its unique energy transfer processes, and more than one energy transfer process may be involved in the upconversion luminescence. Lanthanide-doped UCNPs are comprised of three key components, including a host matrix to embed the lanthanide dopants, a sensitizer or absorber to harvest NIR light, and an activator or emitter to produce upconversion photoluminescence.[38] For example, in the popular $NaYF_4$: Yb, Er/Tm upconversion nanoparticle, $NaYF_4$, Yb and Er/Tm serves as the host matrix, the sensitizer, and the activator, respectively.[39] The energy transfer process of upconversion luminescence for this nanoparticle is illustrated in Fig. 2.

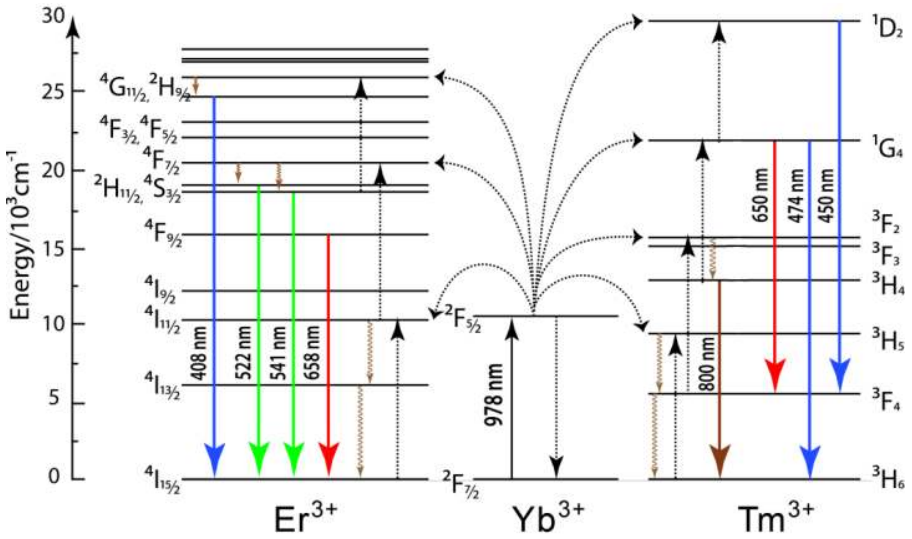

Fig. 2. The energy transfers processes of upconversion nanoparticles co-doped with Yb^{3+}, Er^{3+}/Tm^{3+} under NIR laser irradiation.

As shown in Fig. 2, Yb^{3+} in UCNPs is employed as the sensitizer for Tm^{3+} and Er^{3+} ions co-doped within UCNPs since Yb^{3+} has a large absorption cross-section.[40] Therefore, photon upconversion can be achieved by exciting Yb^{3+} from ground state $^2F_{7/2}$ to its excitation state $^2F_{5/2}$. Following the activation of Yb^{3+}, energy transfer from Yb^{3+} to activators (such as Er^{3+} and Tm^{3+}) occurs. The energy transfer

processes are illustrated in Fig. 2 for Yb^{3+}-Er^{3+} and Yb^{3+}-Tm^{3+} systems. These energy transfer processes thus result in upconversion emissions at 658, 541, 522, and 408 nm for the Yb^{3+}-Er^{3+} system, which are attributed to transitions from $^4F_{9/2}$, $^4S_{3/2}$, $^2H_{11/2}$, $^2H_{9/2}$ to ground state $^4I_{15/2}$, respectively. Similarly, the Yb^{3+}-Tm^{3+} system emits at 800, 650, 475, 450, 362, and 345 nm, corresponding to the radiative transitions from $^3H_4 \rightarrow {}^3H_6$, $^1G_4 \rightarrow {}^3F_4$, $^1G_4 \rightarrow {}^3H_6$, $^1D_2 \rightarrow {}^3F_4$, $^1D_2 \rightarrow {}^3H_6$ and $^1I_6 \rightarrow {}^3F_4$, respectively.[15, 33] The upconversion luminescence emission spectra for both Yb^{3+}-Er^{3+} and Yb^{3+}-Tm^{3+} systems are shown in Fig. 3.

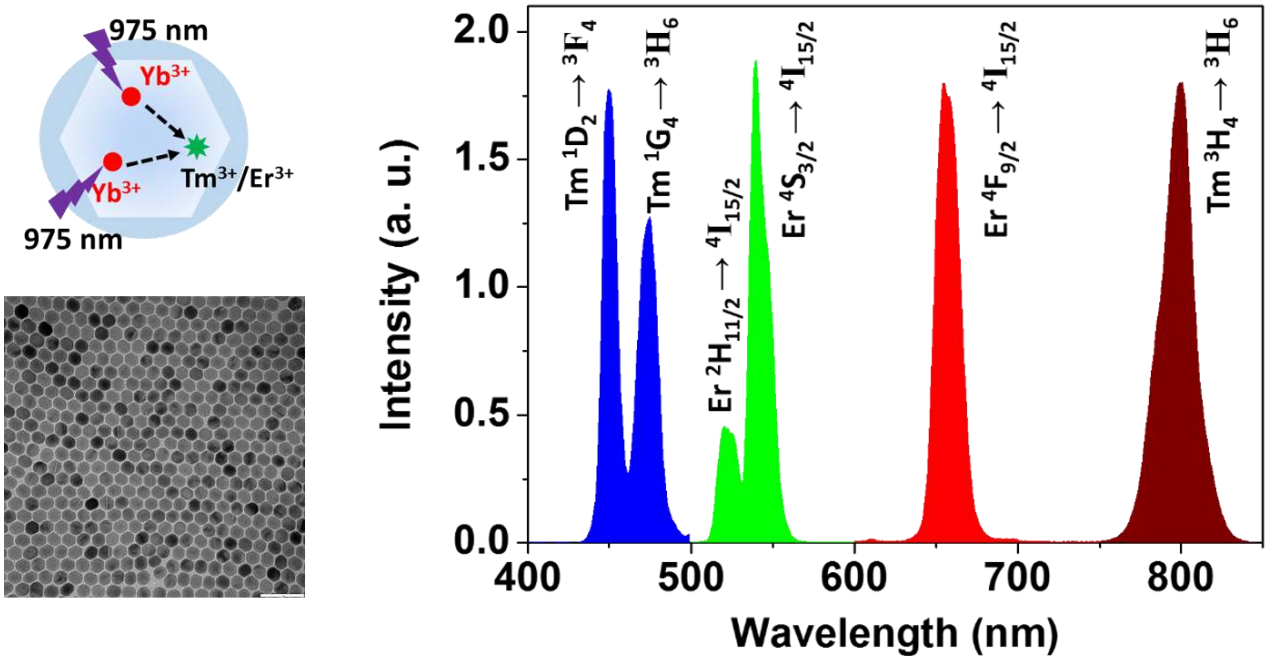

Fig. 3. TEM image (left, scale bar is 100 nm) and luminescence emission spectrum of UCNPs (right), blue (Em = 450 and 475 nm) and NIR emission (Em = 800 nm) from Tm^{3+} doped nanocrystal, and green (Em = 520 and 540 nm) and red emission (Em = 655 nm) from Er^{3+} doped nanocrystal.

2.2. Dye-sensitized UCNPs

Despite the advances of Ln-doped UCNPs, the limitations about the narrow absorption bandwidth of these nanoparticles (excitation wavelength at 980 nm and/or 808 nm laser) impeded the further employment in biomedical applications. Specifically, the parity forbidden nature of 4f-4f transitions of

sensitizers, e.g. Yb^{3+} and a Nd^{3+}-Yb^{3+} pair, resulting in the narrow absorption bandwidth, thus can only harvest a narrow spectral range of incident sunlight and emit low luminescence intensities.[41] To address this limitation, the adequate absorption from NIR light source of the sensitizer, followed by the efficient energy transfer from sensitizer emission to activator absorption, is expected.[42]

Recently, a novel class of dye-sensitized UCNPs has been proposed and explored, and more than 1000 times emission enhancement has been achieved after absorbing laser from broadband spectra.[43] This dye-sensitized upconversion was firstly proposed by Zou and colleagues in 2012.[42] Since then, a variety of studies with respect to the dye-sensitized upconversion nanomaterials have been progressed for the high quantum yield and effective upconversion luminescence. The mechanism of the dye-sensitized upconversion is illustrated in Fig. 4. Within this system, organic dyes, which are attached to the surface of Ln-doped nanoparticles through electronic interaction and physical absorption, and serve as the antenna to harvest the excitation lights. The excitation state of dyes at S1 will then transfer the energy to the sensitizers, such as Yb^{3+} and a Nd^{3+}-Yb^{3+} pair through Föster and Dexter energy transfer.[44-46] Accepting the energy from dyes, the sensitizers are excited, followed by the energy transfer to activators for upconversion emission.

Instead of the Ln^{3+} ions, the energy absorption of dye-sensitized upconversion is dominated by the organic dyes, which are ~1000-10 000 times higher in absorption cross-section.[43] Therefore, efficient upconversion luminescence is then obtained under the excitation at much broader spectral range.

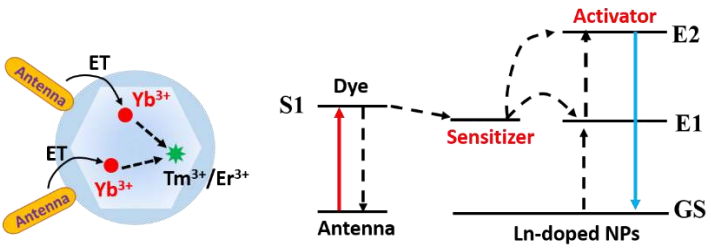

Fig. 4. Schematic illustrations of the mechanisms of dye-sensitized upconversion.

2.3. TTA-based UCNPs

Another upconversion luminescence is triplet-triplet annihilation (TTA).[28, 47-49] Since its first study by Parker and colleagues in 1962, investigations on this upconversion luminescence have attracted much interest, especially in recent years with the successful development of the transition metal complexes-based energy transfer process. The mechanism of the TTA upconversion is illustrated in Fig. 5.[28, 49] Two main parts, namely a sensitizer (energy donor) and an annihilator (energy acceptor), are involved in the process. The upconversion process is initiated via the energy harvesting by the sensitizer, followed by transferring energy to the annihilator to produce upconversion luminescence. In detail, the sensitizer is pumped to excitation state $^1S^*$ upon the light excitation at the power density of mW/cm^2, then the excitation state is populated to its triplet state $^3T^*$ through an intersystem crossing (ISC) with high efficiency.[30, 50] The energy at the $^3T^*$ state of the sensitizer is then transferred to triplet state $^3A^*$ of the acceptor. Repeating this process forms another $^3A^*$ excitation state, which is followed by annihilating these two $^3A^*$ states (TTA) to generate singlet excitation state $^1A^*$ of the acceptor and the subsequent upconversion emission.

TTA-based upconversion luminescence mainly relies on the triplet-triplet energy transfer (TTET) from $^3T^*$ of the sensitizer to $^3A^*$ of the acceptor. The TTET process efficiency: i) is dependent on the lifetime of $^3T^*$ of the sensitizer, typically at microsecond level or longer; ii) is underpinned by TTET between $^3A^*$ of the acceptor and $^3T^*$ of the sensitizer; iii) relies on the distance between $^3T^*$ of the sensitizer and $^3A^*$ of the acceptor, which could be achieved by optimizing the concentration for both sensitizer and annihilator. In addition, the energy level of $^3A^*$ of the acceptor should be lower than that of $^3T^*$ of the sensitizer. Based on these considerations, metal complexes, such as ruthenium (II),[29, 51-53] iridium (III),[54-56] and platinum (II),[57, 58] complexes with long-lived $^3T^*$ states, are normally selected as the sensitizer, and organic π-conjugation molecules are used as the annihilator.

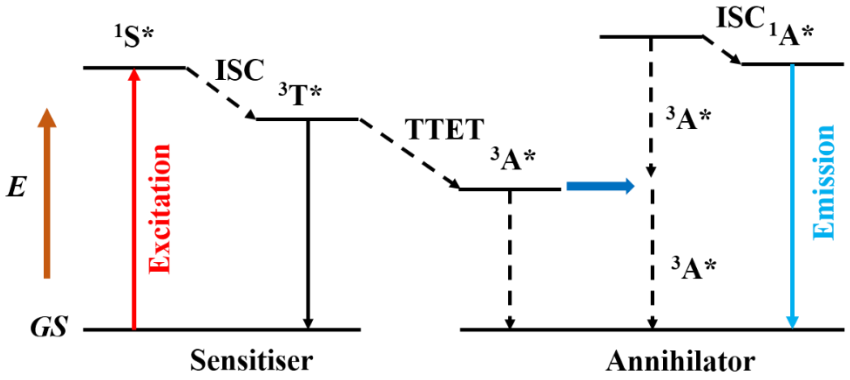

Fig. 5. Jablonski diagram illustrating the TTA-based upconversion process. E: energy; GS: ground state; ISC: intersystem crossing; TTET: triplet-triplet energy transfer; $^1S^*$, $^3T^*$, $^1A^*$, and $^3A^*$: singlet and triplet excitation states of the sensitizer and the annihilator.

3. Control Preparation and biomedical applications of Ln-UCNPs

Ln-doped UCNPs can be excited by long-wavelength radiation (e.g. NIR light) and emit short-wavelength fluorescence through a two-photon or multiphoton mechanism. This unique upconversion process has endowed UCNPs with many optical merits that are desirable in biomedical imaging. Ln-doped UCNPs have deep-tissue imaging capability, narrow emission peaks, large anti-Stokes shifts, controllable luminescence bands, superb photostability, and long lifetime. These excellent optical properties allow UCNPs to be used as a versatile energy transducer to convert NIR light to UV, visible or NIR light. The significant promise of UCNPs in biomedicine has provided the impetus for the development of biofunctional UCNPs in the aspects of synthesis strategies, surface engineering, and application exploration.

3.1 Control preparation of Ln-doped UCNPs

Several synthetic methods have been developed to fabricate lanthanide doped UCNPs, including co-precipitation, thermal decomposition, hydrothermal/solvothermal synthesis, sol-gel method, and ionic liquid-based method. Since biomedical applications favour nanoparticles with small size (typically

<100 nm) and monodispersity, wet chemistry approaches, such as thermal decomposition, and hydrothermal/solvothermal method are widely used in the control preparation of UCNPs for biomedical imaging.

Thermal decomposition method is based on decomposition of lanthanide trifluoroacetate precursor in mixed solvents containing oleic acid (OA), oleylamine (OM), and 1-octadecane (ODE). OA and OM are normally used as surfactants to direct the nanoparticle growth and form surface ligands to prevent nanoparticle aggregation, and ODE with the high boiling point is used as the primary solvent for the synthesis to be conducted at elevated temperatures (250-330 °C). In general, the size and morphology of UCNPs can be well controlled by adjusting the critical synthetic parameters, such as decomposition temperature, reaction time, species and concentration of solvents and the precursor. This synthetic method was firstly introduced by Yan's group and later refined as a most typical and popular route to produce high-quality and uniform UCNPs.[59, 60] So far, this method has been adopted to synthesize a wide range of rare earth metal fluoride, rare earth metal oxide, and rare earth metal oxyfluoride matrix-based nanoparticles with α or β phase structure. Driven by the increasing demand of cellular imaging, the fabrication of sub-10 nm sized UCNPs with high quality has been tailored. To this end, the thermal decomposition method has been carefully adopted to synthesize β-phase UCNPs with the diameter down to sub-10 nm. The successful examples were reported by doping the $NaYF_4$ matrix with a defined concentration of Gd^{3+} ions,[61] controlling the Y^{3+}:F^- ratio and reaction temperature,[62] and replacing Y^{3+} with Lu^{3+} in the nanocrystal matrix.[63]

The hydrothermal/solvothermal synthesis is another well-established and widely used method for the preparation of UCNPs with the uniform shape and size. In a typical process, lanthanide compounds, fluoride salts, and selected surfactants are mixed in solvents. The reaction is performed in a sealed autoclave at the temperature between 160 °C and 220 °C. In this method, the high pressure and temperature conditions help dissolve solid reactants and recrystallize nanomaterials. Surfactants with coordinating capabilities, such as cetyltrimethylammonium bromide (CTAB), ethylenediaminetetraacetic acid (EDTA), and polyethyleneimine (PEI), provide the control over nanocrystal formation and the surface functional groups of the final UCNP product. The morphology,

size, and crystal phase of the resulting nanoparticles can be well tuned by tailing the reaction parameters. This method was introduced by Li's group as a general "liquid-solid-solution" fabrication approach for monodisperse semiconductor, metal, and dielectric nanoparticles, and extended as a sophisticated strategy for the development of UCNPs in water/alcohol/oleic acid mixture with predictable shape and size.[64-66]

Ln-doped UCNPs prepared by the aforementioned methods normally have a considerable number of dopant ions close to the particle surface, therefore, photoluminescence of these Ln dopants are susceptible for quenching by surface ligands or neighbouring solvent molecules that are characterized by high vibrational and phonon energy. As a result, the lanthanide dopants are quenched and the upconversion emission is weakened, which is detrimental for UCNPs in the context of biological imaging and bioanalytical applications. The application of core-shell structures provides an effective solution to minimize the surface quenching, in which the shell is designed to encompass the UCNP core to isolate the dopant ions and surfactant molecules. Moreover, the shell suppresses the energy loss from the UCNP core. An inert shell, such as $NaYF_4$, $NaGdF_4$, or LaF_3, is frequently employed due to the low lattice mismatch with the core composition. For example, the epitaxial growth of $NaYF_4$ (~2 nm) on $NaYF_4$:Yb,Er/Tm resulted in 7.4 times and 29.6 times upconversion emission increase for $NaYF_4$:Yb,Er, and $NaYF_4$:Yb,Tm particles, respectively.[67] An active shell containing Yb ions is also useful in enhancing upconversion emission by promoting the energy transfer from shell Yb ions to core emitters.[68] Another strategy is to increase the number of emitters in a particle by distributing the emitters over several separate layers. For example, 5 mol% Er doped UCNPs in the $NaYF_4$:Yb,Er@$NaYF_4$:Yb@$NaYF_4$:Yb,Er@$NaYF_4$:Yb displayed significantly higher upconversion emission than the typically 2 mol% Er doped UCNPs.[69]

The hydrophilicity and dispersibility in biological buffers are the prerequisites for nanoparticles to be used in most biomedical applications. UCNPs prepared by methods described above are generally hydrophobic owing to the hydrophobic nature of the capping ligands (*e. g.* OA or OM), which greatly limits their application in biomedicine. In order to transfer these hydrophobic nanoparticles into the water, a number of surface modification strategies have been developed, including ligand oxidation,

ligand removal, ligand attraction, ligand exchange, layer-by-layer assembly, and surface silanization (Fig. 6). These surface engineering techniques do not only improve the hydrophilicity and dispersibility of UCNPs in water, but also provide chemically functional groups for subsequent conjugation to biomolecules.

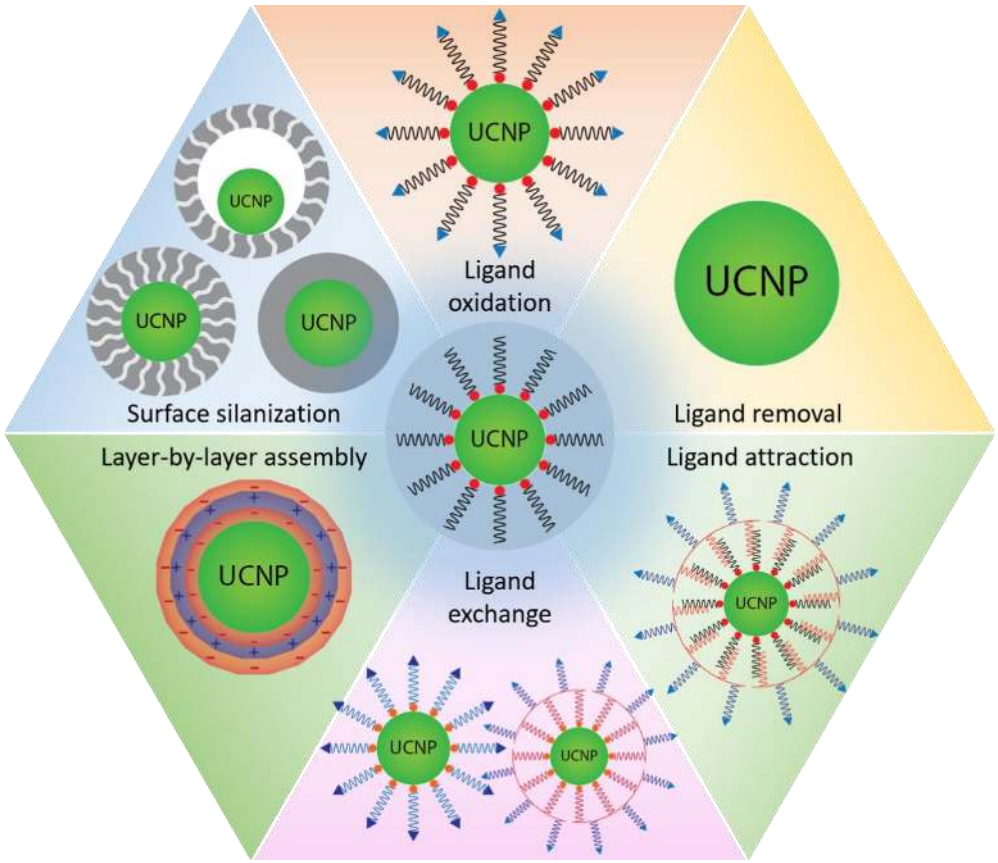

Fig. 6. A diagram of surface modification methods used to alter the surface chemistry of UCNPs.

The unsaturated carbon-carbon double bonds (-C=C-) of OA molecules on the UCNP surface can be directly oxidized to carboxylic acid groups, thereby converting the hydrophobic UCNPs into a water-soluble phase. Li and co-workers firstly reported the ligand oxidation strategy by using the Lemieux-von Rudloff reagent (MnO_4^-/IO_4^-) to oxidize the surface ligand OA into azelaic acids.[70] The carboxylic groups of the resulting azelaic acid do not only provide high dispersibility for UCNPs, but also enables them to conjugate functional biomolecules. In analogy, Yan and co-workers used ozone to oxidize OA into azelaic acid and/or azelaic aldehyde.[71] Their study showed that the oxidation strategy had no

adverse influence on the morphology, crystalline phase, composition and optical properties of UCNPs.[71] This ligand oxidation method is very easy to be implemented. However, it is only applicable to the limited types of hydrophobic surface ligands that have to contain unsaturated carbon-carbon double bonds, and moreover freshly formed azlaic acid seemed to provide insufficient shielding of UCNPs surface from the quenching of water.[72]

Ligand removal is a straightforward strategy to acquire water-soluble UCNPs by removing oleate ligands coated on the UCNP surface. The removal process can be implemented by treating UCNPs with excess ethanol under sonication or simply with strong acid. For example, Xu and co-workers removed OA ligands by washing particles with substantial amount of ethanol assisted by ultrasonication.[73] Alternatively, Capobianco and co-workers dispersed oleate-capped UCNPs with HCl at pH 4 to remove OA and yield hydrophilic UCNPs.[74] At such a low pH, oleate ligand is gradually protonated to form oleic acid and dissociates from the particle, leaving the UCNP naked with lanthanide ions being exposed on the surface.[74] Because of the high surface charge, the obtained UCNPs can be well dispersed in aqueous solutions for a long time. Furthermore, the surface lanthanide ions enable the ligand-free UCNPs to coordinate with molecules that contain functional groups such as -COOH, -OH, -NH_2. To enhance the effective coating of new ligands, Kong and co-workers reported the implementation of a solvothermal processing in the ligand coordination step to form the stronger attachment to the particle surface.[75] It is generally held that the upconversion emission of ligand-coated colloidal UCNPs is increased when compared to ligand-free UCNPs due to the effective shielding of the luminescent core by the new ligands.[74, 76] To impart the biocompatibility to UCNPs, natural molecules, such as polysaccharides, were used to coat on UCNPs via the electrostatic interaction between negatively charged polysaccharides and the surface exposed lanthanide ions of UCNPs.[76]

The ligand attraction method is based on the hydrophobic-hydrophobic interaction between amphiphilic molecules and hydrophobic capping ligands on the UCNP surface to form a second layer of amphiphilic molecules on the UCNP surface. In a typical ligand-attracted UCNP, hydrophobic units

of the amphiphilic compounds interact with the organic capping molecules on the UCNP surface to form an inner interpenetrated layer, while the hydrophilic units facing outwards form the external layer and facilitate dispersion of NPs in aqueous solutions, and provide functional groups for the subsequent bioconjugation. Amphiphilic molecules used in this approach can be modified amphiphilic polymers, block copolymers or surfactants. Using organic synthesis methods, poly(ethylene glycol) (PEG) can be incorporated to provide nanoparticles with improved stability and biocompatibility. So far, poly(maleic anhydride-*alt*-1-octadecene) (PMAO),[77] PMAO-PEG,[78] octylamine-poly(acrylic acid)-poly(ethylene glycol) (OA-PAA-PEG),[79] poly(ethylene glycol)-*block*-poly(caprolactone) (PEG-*b*-PCL),[80] poly((ethylene glycol)-block-lactic acid) (PEG-*b*-PLA),[80] poly(ethylene glycol)-*block*-poly(lactic-coglycolic acid) (PEG-*b*-PLGA),[80] polyethylene glycol *tert*-octylphenyl ether (C_8PhE_{10}),[81] and phospholipids[82] have been reported to be successfully attracted by UCNPs and render the particles hydrophilic. Due to the presence of PEG, the resulted nanoparticles form stable dispersions for more than a week in water or buffers.[80, 81, 83] As alternatives to PEG, other stealth polymers, poly(amino acids)[84] and poly[*N*-(2-hydroxypropyl)methacrylamide,[85] and zwitterionic polymers[86] have also been investigated to form highly stable UCNPs via the ligand attraction method. The colloidal stability and the upconversion luminescence of modified UCNPs are highly dependent on the structure of the amphiphilic polymer, in which the relative length of the hydrophilic to hydrophobic part plays an important role. The higher ratio of the hydrophilic to hydrophobic parts increases the hydrophilicity of the copolymer coated on UCNPs, and hence the better disposability in water.[87] As quenching of the upconversion luminescence is mainly attributed to the contact of water molecule with UCNPs, the length and compactness of the hydrophilic chains determined the shielding of the nanoparticle surface from the aqueous environment. It is therefore believed that amphiphilic polymers with a higher ratio of hydrophilic-to-hydrophobic part results in dense packing of the hydrophilic outer layer on UCNPs, hence brighter UCNPs.[87]

Ligand exchange is a physicochemical process, in which original hydrophobic capping ligands on the UCNP surface are replaced with new binding molecules. Usually, the new binding molecules should have functional groups that allow them to firmly anchor on the UCNP surface along with hydrophilic

tails to provide water dispersity and functionality. A variety of molecules have been used to decorate UCNPs with hydrophilic moieties, including polyacrylic acid (PAA),[88] hexanedioic acid,[89] 6-aminohexanedioic acid,[90] 3-mercaptopropionic acid,[91] PEG-diacid,[92] citrate,[93] PEG-phosphate,[94] 2-aminoethyl dihydrogen phosphate,[95] phosphate modified DNA,[96] poly (amidoamine) (PAMAM),[97] PEI,[98] poly(allylamine),[99] polyvinylpyrrolidone,[100] and tetramethylammonium hydroxide (TMAH).[101] Recently, Marray and co-workers reported a versatile ligand exchange method using nitrosonium tetrafluoroborate ($NOBF_4$) to replace the original surface ligands at room temperature, thereby stabilizing UCNPs in aqueous solutions.[102] The intermediate nanoparticles ($NOBF_4$-UCNP) can be then subject to further surface manipulation by replacing $NOBF_4$ with desired surface molecules for subsequent bioconjugation.[102] The long-term stability of UCNPs after ligand binding is crucially determined by the stability of the ligand coordination with lanthanide ions. Therefore, multidentate ligands, such as polymers and dendrimers with a number of coordinating atoms, are preferred over monodentate molecules.[89] In addition, the ligand with functional groups such as phosphate (four coordination sites),[103] sulphonate (three coordination sites),[104] or carboxylate (two coordination sites)[72] groups shows stronger coordination capability than amine groups towards UCNPs.

Layer-by-layer assembly employs the electrostatic interaction between species with opposite charges to coat the charged surface of UCNP. Polyanions (*e.g.* PAA) and polycations (*e.g.* PEI) are normally used in this method for alternate deposition on the UCNPs surface.[105] The deposition process is mainly performed in a solution by repeated incubation and washing. Hence, this method is simple and versatile in controlling the hydrodynamic size and surface charge of the obtained UCNPs. Moreover, desired functional groups can be incorporated to the UCNP surface for biomolecule conjugation. Li and co-workers modified UCNPs by depositing positively-charged polymer, poly(allylamine hydrochloride) (PAH), and negatively charged polymer, poly(styrene sulfonate) (PSS), sequentially on the negatively charged UCNPs to generate PAH/PSS/PAH UCNP nanocomposites.[106] The outmost polymer layer provides abundant reactive groups that enable coupling with molecules for biomedical applications.

Silica-coating with further surface functionalization is another popular method to modify UCNPs. Silica has been widely used for nanoparticle coating due to its rich surface chemistry, controllable pore

size, biocompatibility, optical transparency, and chemical stability. The surface chemistry of silica can be easily tuned by organofunctional alkoxysilane molecules via self-assembly. As a result, coating a silica shell on the UCNP surface is able to stabilize the particles in various buffers and provide an amenable surface for easy add-on of functionalities (-NH_2, -COOH, or -SH). Silica-coating is applicable to both hydrophobic and hydrophilic UCNPs via the reverse microemulsion method or Stöber method.[107, 108] Besides coating of a dense silica layer ($dSiO_2$), many groups have also devoted efforts to grow mesoporous silica ($mSiO_2$) shell or hollow mesoporous silica ($hmSiO_2$) on the UCNP surface in an attempt to use the nanocomposite as delivery vehicles.[109] The unique porous or rattle structure of $mSiO_2$ and $hmSiO_2$ is particularly useful in biomedical applications, when high loading of analytical or therapeutic materials is required. The mesoporous structure can be achieved by adding a micelle-forming reagent (such as CTAB) during formation of the silica shell. The micelles are then removed by washing the colloid with a solvent of suitable pH or by refluxing particles.[110] Compared with $mSiO_2$, the $hmSiO_2$ coating provides the larger accommodation volume for drugs due to the presence of voids between the UCNP core and mesoporous shell. The $hmSiO_2$ coating method was recently developed by Shi and co-workers, in which they coated two layers of $dSiO_2$ on a hydrophobic UCNP, followed by etching the first $dSiO_2$ shell along with generating mesopores in the second silica shell, yielding a rattle structure.[111] Although silica coating has been proven to be an effective surface modification strategy, the formation of dispersible and long-term stable nanoparticles is difficult. For example, more than one nanoparticles can be encapsulated by a single layer of silica, leading to enlarged particle size and polydispersity.[112] Additionally, the dispersion of silica-coated UCNPs exhibits poor stability in aqueous solution and buffers since the nanoparticles have a propensity to aggregate and precipitate within a few hours.[113, 114]

3.2 Biomedical applications of Ln-UCNPs

In recent years, the design of multifunctional UCNPs for diverse applications has attracted intensive interest, especially in the field of biomedicine.[115, 116] Since UCNPs can be used as promising imaging contrast agents, various UCNP-based nanocomposites have been explored for imaging cells,

organs/tissues and animals, detecting analytes, delivering drugs, mediating photodynamic therapies, and tracking delivery process. Furthermore, enhanced upconversion luminescence from Tm-doped UCNPs ($NaYF_4$:Yb, Tm) has been found at the high power laser excitation for the higher concentration of Tm^{3+} doping.[117] When this high Tm-doping UCNPs were excited under both 980 nm and 808 nm, the blue luminescence was optically inhibited. Based on this property, higher Tm^{3+} doping UCNPs have been successfully applied in low-power super-resolution stimulated emission depletion (STED) nanoscopy.[118] In this section, the application of UCNPs in bioimaging, bioanalysis and theranostics is thus summarized.

3.2.1 Bioimaging

Conventional fluorophores (organic dyes, luminescent metal complexes, fluorescent proteins, and quantum dots) experience many limitations in the photoluminescent imaging, such as high background noise from tissue autofluorescence, photobleaching, and photodamage to biological samples. These drawbacks associated with *in vitro* and *in vivo* fluorescence imaging can be overcome by using UCNPs. A particularly useful type of UCNPs is co-doped with Yb^{3+} and Tm^{3+}, which emits NIR photoluminescence in the range of 750-850 nm under 980 nm excitation. The excitation and emission wavelengths of these NIR-to-NIR UCNPs lie in the optical transparency window of the biological tissue. Therefore, these UCNPs can allow for minimal autofluorescence and light scattering from the tissue, leading to an ultrahigh imaging contrast. For example, Li reported the high-contrast targeted imaging of a nude mouse bearing human glioblastoma U87MG tumors using RGD peptide conjugated $NaYF_4$:Yb,Tm.[119] The signal-to-noise ratio between the labeled tumor and background was determined to be ~24.[119] Another fascinating feature of NIR-to-NIR UCNPs is their capability of deep tissue imaging. Recently, Prasad and co-workers developed a NIR-to-NIR core-shell $NaYbF_4$:Tm@CaF_2 UCNP for the whole body photoluminescent imaging of mice,[120] as shown in Fig. 7. They obtained an extraordinarily high signal-to-noise ratio of 310 using these UCNPs for *in vivo* imaging. Remarkably, the fluorescence signal from UCNPs can still be detected and imaged under 3.2-cm thick pork tissues.[120] This depth imaging will be of great use for *in vivo* and clinical imaging.

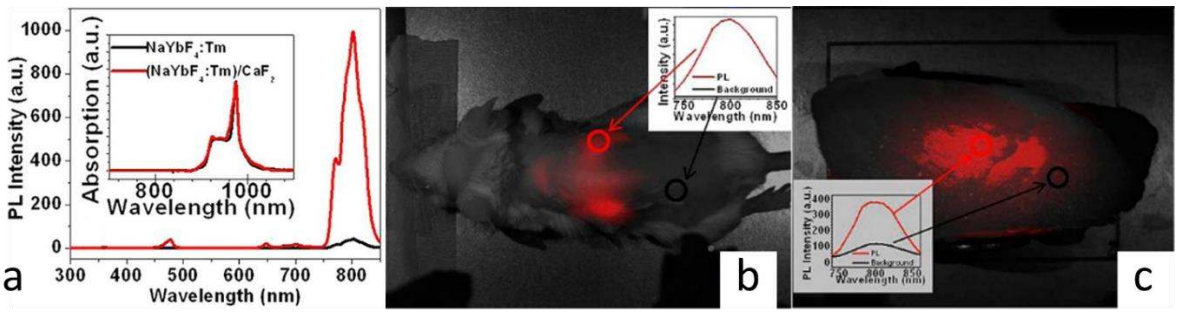

Fig. 7. (a) Upconversion photoluminescence spectra of core ($NaYF_4$:Tm) and core-shell ($NaYF_4$:Tm@CaF_2) UCNPs under NIR illumination. (b) Imaging of a BALB/c mouse injected with the hyaluronic acid modified core-shell UCNPs through tail vein injection. (c) Photoluminescent image of the cuvette containing core-shell UCNPs covered with a piece of 3.2-cm pork tissue. Reprinted with permission from ref. 120. Copyright 2012 American Chemical Society.

In addition to photoluminescent imaging, imaging contrast for other imaging modalities, such as magnetic resonance imaging (MRI), computed tomography (CT), positron emission tomography (PET) can be introduced into UCNPs to develop UCNP-based multimodal imaging probes. For instance, Gd^{3+} was co-doped in the UCNP host matrix and used as a core or shell material in the core-shell UCNPs for the fabrication of a nanoprobe for optical and MRI dual imaging.[121] Lu^{3+} ion, having the highest atomic number among the lanthanide elements, is recently considered as the new matrix material ion in developing UCNPs ($NaLuF_4$) for CT imaging, showing higher contrast capability than that of the commercial iodinated agents.[122] PET radioactive ions such as $^{18}F^-$ can be incorporated into a $NaYF_4$ matrix via the cation assisted ligand assembly, resulting in ^{18}F-labeled UCNPs for both photoluminescent and PET imaging.[123]

3.2.2 Bioanalysis

Being excited by NIR light, UCNPs circumvent autofluorescence and light scattering from biomolecules and tissues, which provides a promising imaging platform for the use in bioanalytical

applications. Over the past years, UCNPs have been widely employed to construct nanoprobes by integration with recognition molecules for biosensing applications.[124, 125] The sensing mechanism of such UCNP-nanosensor is based on either inferring filter effect or luminescence resonance energy transfer (LRET).[126] In the first case, the luminescence intensity of UCNPs is decreased when the upconversion emission is reabsorbed by analyte molecules during detection. The concentration of analytes is determined by their filter effect of UCNPs. In the second case, UCNPs are used as the energy donor and coupled with an acceptor to form a LRET pair, wherein the energy is transferred nonradiatively from UCNP to the acceptor molecule under NIR excitation. Such energy transfer will result in changing the intensity of one upconversion emission band or intensity ratio of two bands, which is correlated with the spectral overlap and distance between the energy pair. By manipulating LRET between UCNPs and acceptor molecules, high sensing efficiency can be achieved. Based on these two sensing strategies, UCNP biosensors have been used to detect biomolecules, gas molecules, and the temperature in biosystems.

Recently, Li's group has produced a series of UCNP-based nanoprobes by assembling the ion responsive agent with UCNPs.[63, 127, 128] In a typical example, they reported the binding of a CN^- responsive complex, chromophoric iridium (III), to the green- and red-emitting UCNPs to produce a ratiometric luminescence probe for CN^- detection.[127] As shown in Fig. 8, the interaction of CN^- anions with Ir1 led to the decrease of adsorption of Ir(III) complexes. As the result, the energy transfer from UCNP to the chromophoric iridium complex was inhibited, leading to the recovery of green emission of UCNPs.[127] Using a specific interaction between molecules, such as biotin and avidin, antibody and antigen, aptamer and receptor, DNA hybridization, detection of biomolecules with high sensitivity and specificity can be achieved via the inhibition or promotion of the energy transfer between UCNP and the acceptor.[129, 130] In addition, Zhang et al. developed UCNP-based DNA via conjugating the capture oligonucleotide to green-emitting UCNPs and using an intercalating dye SYBR Green I as the energy acceptor to quench the emission of UCNPs.[131] Once hybridization occurs between the target and capture oligonucleotides, green emission of UCNPs is transferred to SYBR Green I, resulting in the luminescence drop of UCNPs and emission increase of SYBR Green I.[131]

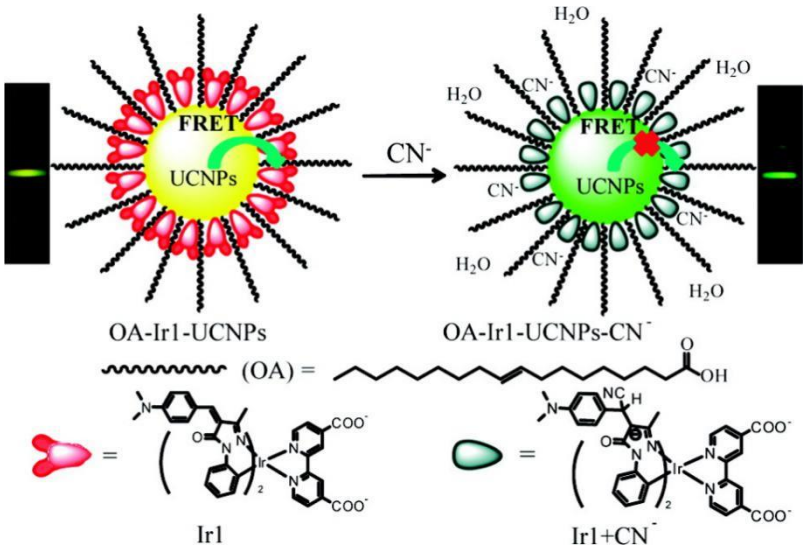

Fig. 8. Recognition mechanism and the LRET process of Ir1-UCNPs towards CN^-. Reprinted with permission from ref. 127. Copyright 2011 American Chemical Society.

3.2.3 Therapeutic applications

Light-stimulated drug delivery and therapeutic effect are a popular means in biomedicine due to the focused positioning, easy manipulation, and high selectivity. Compared to the conventional drug delivery and therapeutic systems using UV or visible lights, the UCNP-based therapeutic system can be activated by NIR irradiation, and therefore avoid the drawbacks of shallow tissue-penetration depth of light and photodamage to biological tissues.[132] NIR-controlled drug delivery systems based on UCNPs are designed to manipulate the release of drugs via NIR irradiation or to activate the therapeutic effect of prodrugs within the diseased sites.[133] UCNPs are generally integrated with therapeutic reagents and photolabile protecting molecules or photoswitchable molecules that can cage drugs inside the nanocarrier. Upon irradiation with the appropriate wavelength, the caged drugs are released after photolysis of the protecting molecules or through the mouth opening by photoswitchable molecules. In the UCNP delivery system, UCNPs serve as a powerful NIR light converter to transform NIR irradiation into UV or visible emission that drives the photoreaction of these compounds.[132] The control of the drug release can be achieved by tuning the power intensity and irradiation time of the excitation light. For

instance, Shi and co-worker developed a novel NIR-triggered photosensitive carrier by encapsulating azobenzene (azo) groups and DOX inside the mesopores of the silica layer on $NaYF_4$:Yb,Tm@$NaYF_4$@mSiO_2.[134] In their fabricated nanocomposites, the *trans* isomer of azo molecules will transform into the *cis* isomer by UV upconversion emission, whereas the *cis* isomer will reverse to the *trans* isomer again when excited with visible upconversion emission.[134] This back-and-forth wagging motion of azo molecules is responsible for impelling the release of DOX, and the release amount of DOX can be readily controlled by the NIR power density and irradiation duration.[134]

Besides drug delivery, UCNPs have also shown great promise in the application of photodynamic therapy for deep-tissue treatment.[54, 135] In the UCNP-based nanocomposite loaded with photosensitizers (PSs), UCNP is capable of converting the deep-penetrating NIR to UV/visible light under the relatively low excitation intensity (<1 W/cm^2), thereby initiating the therapeutic effect from the surrounding PSs.[26, 136] NIR irradiation affords the higher accessibility towards the deep tissue, thus providing a possibility of treating deep-seated tumors. The multiple emission and optical tunability of UCNPs provide additional benefits to match absorption of PSs and excite two or more types of PSs in one nanoplatform to attain higher therapeutic efficiency.[114]

4. Design of dye-sensitized UCNPs for biomedical applications

As a new strategy of upconversion process, dye-sensitized upconversion has shown many superiorities, such as significantly higher emission intensity with lower excitation power and broader excitation wavelength. These optical properties endorse the utility of dye-sensitized UCNPs in the biomedical applications, such as bioimaging and treatment. The research focus of dye-sensitized UCNPs is mainly in the screening of different organ dyes as the sensitizer. In this section, the methods for the design and preparation of dye-sensitized UCNPs, strategies for enhancing luminescence and bio-availability and biomedical applications are summarized.

4.1 Strategies for the design of dye-sensitized UCNPs

The key component of the design strategy for dye-sensitized UCNPs lies on the selection of organic dyes as the antenna. Spectral overlapping and the critical distance between the selected dyes and sensitizers are the two factors, normally being followed to maximize the ET efficiency. Since the first description of IR 806-sensitized upconversion in 2012 by Zou and colleagues, several organic dyes have been recently reported and employed as the antenna.[42, 43, 137] These organic dyes for the dye-sensitized upconversion can be classified as single dye- and multi dye-dominated energy cascaded upconversion.

4.1.1. Single dye-dominated energy-cascaded upconversion

Most reported strategy for the design and preparation of dye sensitized UCNPs is based on the single dye energy cascade process. Except for IR-806, Han et al. reported that other organic dyes, including IR-783, IR-808, IR-820, IR-845 can capture various bands of NIR photons for subsequent energy transfer to Ln-sensitizers for upconversion [138]. Indocyanine green (ICG), a commercial organic dye with emission at 840 nm under 800 nm irradiation, has also been explored as the antenna for energy transfer for upconversion.[139] To alleviate the concentration quenching of ICG, the Nd^{3+} doped colloid nanoparticles, $NaYF_4$:Nd were prepared to facilitate the nonradiative energy transfer from ICG to Nd^{3+}.[140] The energy transfer efficiency was determined to be 57%, ~10 times enhancement in upconversion luminescence [140]. Upconversion based resonance energy transfer network is then reported by Laboda *et al.*. [44] Cyto 840, attached to $NaYF_4$:Yb, Tm, served as the antenna in this network. Being excited at 810 nm laser, the energy transfer occurred from S_1 state of Cyto 840 to Yb^{3+} for upconversion. Assembling of another dye, ATTO 488 in this network, subsequent energy transfer can be obtained from $NaYF_4$:Yb,Tm to ATTO 488.[44]

Enhancing the upconversion luminescence and photothermal conversion properties has been obtained with a dye-sensitized core/shell nanoparticle. Within such a system, the IR-806 was employed as the antenna for the subsequent energy transfer to Nd^{3+}, Yb^{3+} in the shell, and then Yb^{3+} and Er^{3+} in

the core. A maximum enhancement by 28 times in the upconversion luminescence was achieved with this organic-inorganic core-shell nanoparticle.[137]

4.1.2. Multi dyes co-sensitized upconversion

Compared to the single dye-dominated dye sensitizing, multi dye co-sensitized upconversion processes have less been reported, but own highly potential superiorities in terms of broad spectral absorption and the intensity of upconversion luminescence. Chen *et al.* reported that the dye-sensitized upconversion luminescence can be obtained by attaching two dyes, IR-808 and IR-820, to a core/shell nanoarchitecture, $NaYF_4:Yb^{3+},Tm^{3+}$ (0.5%)@$NaYF_4:Nd^{3+}$ (30%).[141] The upconversion quantum efficiency was determined to be 19%, with the upconversion energy transfer efficiency of 9.3% and the upconversion quantum yield of 4.8%.[141] Multi dye sensitized upconversion can be also achieved by absorbing lights from more broad spectral range from blue to NIR. Three dyes, BODIPY-FL, Cy3.5, and IR-806 with different absorption capacity were employed as sensitizer I, II, and III, respectively.[142] The energy harvested by sensitizer I can transfer to sensitizer II, followed by the sequential energy transfer to sensitizer II, sensitizer III, Yb^{3+}, and then Tm^{3+} activator of NaYF4:Yb^{3+},Tm^{3+}. In addition, irradiation of anyone of three sensitizers can trigger the multi-step cascade energy transfer, extending the absorption band of upconversion with the energy transfer mechanism.[46]

4.2 Biomedical applications of dye-sensitized UCNPs

4.2.1. Bioimaging

Unique luminescence properties of dye-sensitized UCNPs allow themselvesto be used in bioimaging. In a core-shell-shell nanocrystal, ICG was attached to the surface of $NaYF_4:Yb^{3+},X^{3+}$@$NaYbF_4$@ $NaYF_4:Nd^{3+}$ (X = null, Er, Ho, Tm, or Pr) as the antenna (Fig. 9A).[139] The energy captured by ICG was then transferred to Nd^{3+}, Yb^{3+}, and then Yb^{3+}, X^{3+} for upconversion emission. An enhancement by ~4 times in upconversion luminescence was achieved.[139] Co-coating the surface of this core-shell-shell nanocrystal with ICG and an amphiphilic polymer, 1,2-distearoyl-sn-glycero-3-phosphoethanolamine-

N-[methoxy(polyethylene glycol)-2000] (DSPE-PEG-2000), the nanoparticles were transferred into water solution. This water soluble nanoparticle was then subcutaneously injected into a mouse with a depth of ~3 mm. Results showed clear luminescence signal under 800 nm laser irradiation (Fig. 9B).[139]

Cy7 has also been explored as the antenna for dye-sensitized upconversion through a sequential Cy7-Nd^{3+}-Nd^{3+}-Yb^{3+}-Er^{3+} energy transfer. Approximately 17 times enhancement in upconversion luminescence was obtained under 800 nm laser irradiation. Using phosphatidylcholines as the surfactant, Zou *et al*. coated Cy7 on the surface of $NaYF_4$:Yb^{3+},Nd^{3+}@$NaYF_4$:Nd^{3+} core-shell nanocrystal.[143] This water dispersible nanoparticle showed enhanced sensitizing upconversion luminescence, which was further used in imaging in living HeLa cells and lymph of mice.

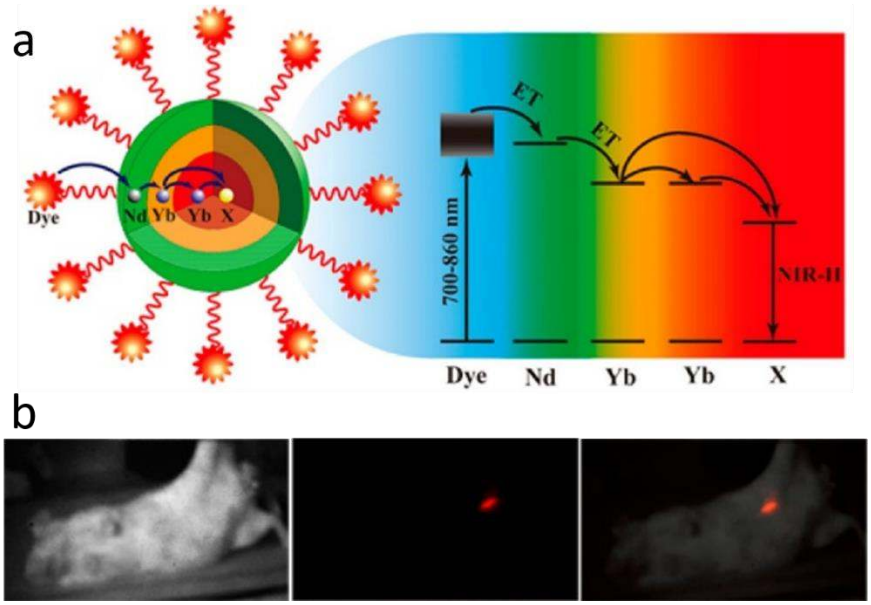

Fig. 9. (a) Energy transfer pathway from ICG on the surface of $NaYF_4$:Yb^{3+},X^{3+}@$NaYbF_4$@$NaYF_4$:Nd^{3+} nanocrystal, to the Nd^{3+} ions in the outer shell, then to the Yb^{3+} in the inner shell, and finally to the Yb^{3+},X^{3+} (X = null, Er, Ho, Tm, or Pr) in the core, producing large Stokes-shifted NIR-II emissions. (b) NIR-II photoluminescent bioimaging of a mouse with subcutaneous injection (excited at 800 nm). Reprinted with permission from ref. 139. Copyright 2016 American Chemical Society.

Wu *et al*. also reported an IR-806 sensitized upconversion nanocomposite, where IR-806 was employed as the antenna.[144] Upon irradiation with an 800 nm continuous laser, the dye-sensitized upconversion emission was noticed as the efficient energy transfer from IR-806 to Yb^{3+} sensitizers. Core-shell nanostructures, $NaYF_4:Yb^{3+},Er^{3+}@NaYF_4$ and $NaYF_4:Yb^{3+},Er^{3+}@NaYbF_4$ exhibited enhanced sensitizing luminescence emission than core alone. Surface encapsulating of $NaYF_4:Yb^{3+},Er^{3+}@NaYbF_4$ with IR-806 and surfactant, Pluronic F-127, water-dispersed nanoparticles were obtained with enhanced sensitizing upconversion luminescence. Bioimaging application *in vivo* of such a dye-sensitized upconversion was further demonstrated.[144]

4.2.2. Phototherapy

Dye-sensitized upconversion has also been involved in photodynamic therapies, an emerging therapeutic modality for cancer treatment. Recently, Xu *et al*. reported the first attempt to use the dye-sensitized upconversion as the light to activate the photosensitizers locally within a mesoporous silica nanoparticle.[145] Within this system, IR-806 was employed as the antenna to capture the near infrared light from 808 nm laser. The upconversion was then obtained through a multi-step cascade energy transfer process, *i. e.* dye-Nd^{3+}-Yb^{3+}-Er^{3+} in an IR-806 coated $NaGdF_4:Yb^{3+},Er^{3+}@$ $NaGdF_4:Nd^{3+},Yb^{3+}$ core-shell nanostructure (Fig. 10a, b).[145] Two photosensitizers, Ce6 and MC540, were loaded into the mesoporous silica shell through chemical conjugation and adsorption, respectively. Under 808 nm laser irradiation, a lot of reactive oxygen species were obtained for tumor ablation (Fig. 10c, d).[145] In contrast, upon radiation with the 980 nm laser, the photosensitizing by dye-sensitized upconversion showed lower ablation effects.[145]

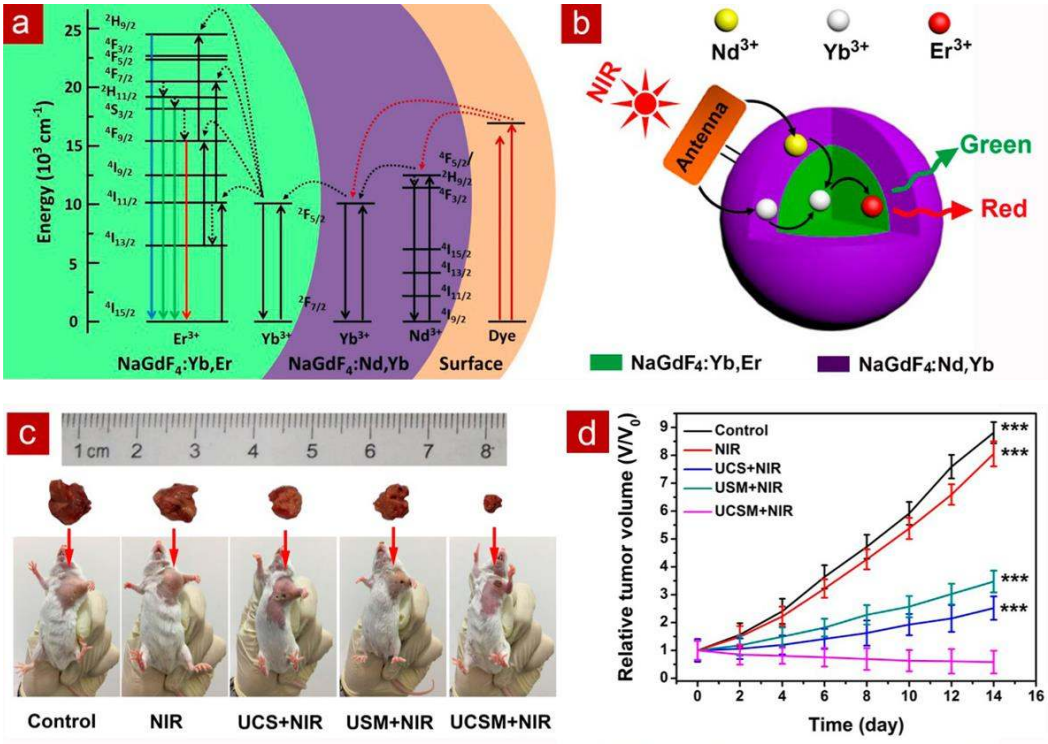

Fig. 10. Schematic illustration of the energy level diagram (a) and the energy transfer mechanisms in dye-sensitized upconversion upon 808 nm excitation (b). Photographs of mice and excised tumors from representative mice (c); and changes in the relative tumor volume (d) achieved from mice with varying treatments. Reprinted with permission from ref. 145. Copyright 2017 American Chemical Society.

5. Construction of TTA-based UCNPs for biomedical applications

Although Ln-doped UCNPs have been successfully applied in the biological systems, the biomedical application may be hampered by their intrinsic drawbacks, such as low absorption cross-section of the sensitiser, low quantum yield, and high excitation power density. Different with Ln-UCNPs, recently studies on the TTA-based upconversion showed high emission quantum yield at low power laser excitation, which enable the developed TTA-UCNPs to be developed for bioapplications. Together with the excitation at the NIR range with higher penetration depth for biological samples, this intense upconversion emission allows them to be potentially used as the upconversion luminescence probes for optical bioimaging. Currently, TTA-based upconversion research mainly focuses on the development of sensitizer molecules, while the biological applications of TTA-based UCNPs have rarely been

reported. Even so, as one of the most important upconversion processes, current advances in the development of TTA-based UCNPs for biomedical applications are summarized in this review. There are two types of nanomaterials that have been reported, including soft encapsulating and rigid nanomaterials.

5.1. Soft encapsulation

Soft encapsulating refers to entrapping both sensitizer and annihilator molecules in a soft material environment, such as nanocapsules and micelles.[146, 147] The sensitizer and annihilator of TTA-based UCNPs are normally hydrophobic molecules,[148] which can be well dispersed in a non-polar solvent or oil. This hydrophobic microenvironment does not only serve as the solvent for the sensitizer and annihilator, but also protect their triplet state of $^3T^*$ and $^3A^*$ from oxygen quenching, increasing the upconversion efficiency. Functional hydrophilic surface endows the prepared UCNPs with biocompatibility and water dispersibility for further biological applications.

Wohnhaas *et al*. used polymeric nanocapsules as the matrix to prepare TTA-based UCNPs.[149, 150] The sensitizer (2, 7, 8, 12, 13, 17, 18-octaethylporphyrinato) Pd(II) (PdOEP) and the annihilator (perylene) were embedded into the nanocapsules during polymerization. The prepared nanoparticles showed well-defined core-shell structure (10-20 nm shell thickness under transmission electronic microscope). The size of the polymeric nanocapsules was in the range of 75-100 nm (hydrodynamic radius, 20% standard deviation).[149] Upon laser excitation at λ_{ex} = 532 nm (on the level of 0.05W/cm^2), intense upconversion luminescence was obtained for perylene at λ_{em} = 433 to 481 nm. Using these upconversion nanocapsules, imaging of malignant cells was demonstrated and the cellular uptake mechanism was investigated. Polymer nanofibers were also prepared by simultaneously electrospinning aqueous polymeric solution with pronounced oxygen-barrier properties and functional nanocapsules containing meso-tetraphenyltetrabenzoporphyrin palladium (PdTBP) and 1,3,5,7-tetramethyl-8-phenyl-2,6-diethyl dipyrromethane•BF2 (dye550) as the sensitizer/emitter couple.[151] This fiber showed efficient upconversion fluorescence centered at λ_{em} = 550 nm under low intense excitation with a

continuous wave laser (λ_{ex} = 635 nm, power = 5 mW). Under oxygen-free atmosphere, Katta *et al*. synthesized a TTA-upconversion polymeric nanocapsule by free-radical micoremulsion polymerization in darkness.[152] With this procedure, oxidation of annihilator molecules by singlet oxygen, generated during the synthesis in daylight conditions and the oxygen-rich environment was minimized. As a result, the prepared PdOEP-perylene nanoparticles showed intensive upconversion emission at λ_{em} = 470 nm with excitation at λ_{ex} = 532 nm (excitation intensity was tens of mW/cm^2).

Polymeric TTA-upconversion nanocapsules were also fabricated as the photocontrolled cell binding agent. By exploiting the mechanisms of TTA-upconversion and Förster resonance energy transfer (FRET), Wang *et al*. created an upconversion-based photoresponsive system (Fig. 11).[153] In this system, sensitizer and annihilator molecules, PDOEP and 9, 10-diphenylanthracene (DPA), were encapsulated into a hydrophobic core of polymeric micelle that was self-assembled from the block copolymer poly($_{D,L}$-lactic acid)-poly(ethylene oxide) (PLA-PEG). The tumor cell targeting peptide, cyclo-(RGDfK) was caged by photocleavable coumarin group (DEACM) and bound to the PLA-PEG chain. Upon the laser excitation at λ_{ex} = 532 nm, cleavage of the DEACM by upconversion emission from DPA reactivated cyclo-(RGDfK), allowing tumor cell targeting.

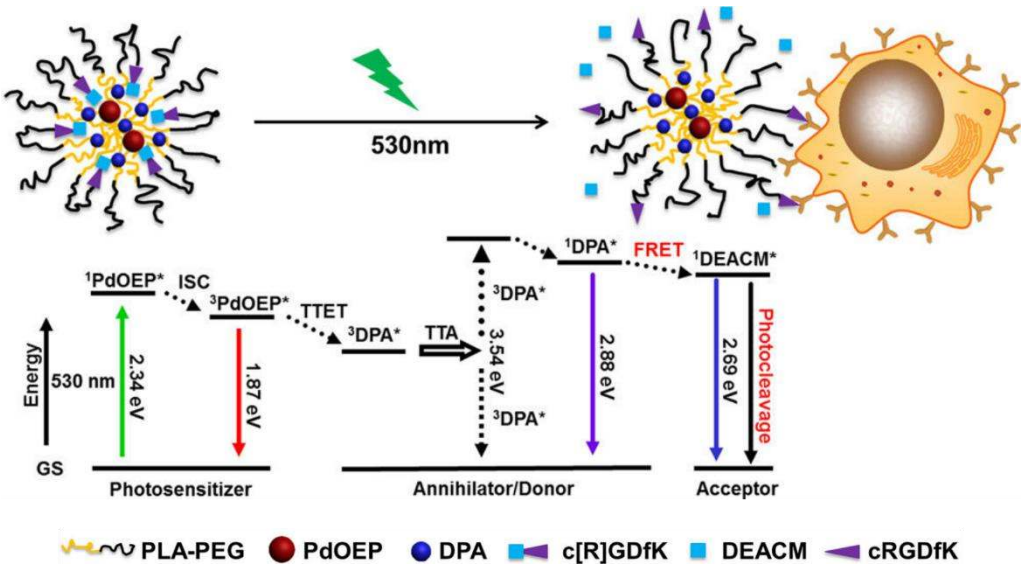

Fig. 11. Schematic illustration of the photoactivatable TTA upconversion nanoparticle for tumor cell targeting (top). Jablonski diagram illustrating the mechanism of TTA-UC and FRET processes (bottom). Reprinted with permission from ref. 153. Copyright 2015 American Chemical Society.

Bovine serum albumin (BSA)-dextran stabilized soybean oil was also exploited as the soft material for the development of TTA-based UCNPs for bioimaging (Fig. 12).[154] Dispersion of the sensitizer and annihilator molecules, Pt(II)-tetraphenyl-tetrabenzoporphyrin (PtTPBP) and BODIPY derivatives (BDP-G and BDP-Y with the maximal fluorescence emission at 528 and 546 nm, respectively) in soybean oil does not only protect the quenching from oxygen, but also ensures high translational mobility of BDP-G and BDP-Y, allowing less quenching by aggregation. Under the 635 nm laser irradiation, the upconversion efficiency was 1.7% and 4.8% for UCNP-G, and UCNP-Y, respectively. By virtue of high upconversion efficiency of these nanoparticles, lymph node luminescence imaging of living mice *in vivo* was successfully demonstrated under low-power density excitation (12.5 mW/cm^{-2}). Similar BSA stabilized upconversion nanocapsules were also developed by Tian and colleagues.[155] In this UCNP, PtPBP excitable at 635 nm and a boron dipyrromethene derivative (BDP) with the emission center band at 558 nm were selected as the sensitizer and annihilator, respectively. The prepared UCNPs showed excellent stability, low cytotoxicity, ensuring the following biological imaging in cells and mice.

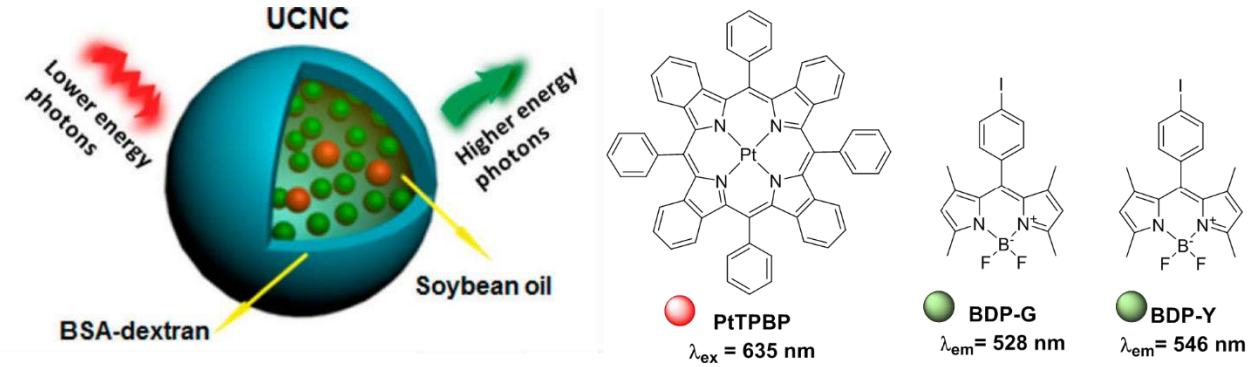

Fig. 12. Schematic illustration of TTA upconversion process of the upconversion nanocapsules (UCNC), and chemical structures of sensitizers (PtTPBP) and annihilators (BDP-G, and BDP-Y). Reprinted with permission from ref. 154. Copyright 2013 American Chemical Society.

Micelle was also explored as the carrier for embedding both sensitizer and annihilator molecules for TTA-based upconversion.[156] UCNPs with the diameter of 30-35 nm were produced by incorporating the sensitizer and annihilator pair, PdTBP/perylene, in micelles. Under the excitation at λ_{ex} = 635 nm, UCNPs showed intense upconversion luminescence from perylene at λ_{ex} = 450 nm. Unfortunately, all the spectrometric measurements were conducted in oxygen-free conditions, leading to less possibility for the biomedical applications.

5.2. Rigid shells

The development of rigid nanomaterials for TTA-based upconversion mainly focuses on encapsulating both sensitizer and annihilator molecules in a silica nanoparticle.[157-159] By loading Pd complex octaethylporphyrin (PdOEP) and DPA into a silica nanoparticle, TTA-based UCNPs were successfully fabricated by Liu and colleagues.[160] TTA UCNPs showed high upconversion efficiency (4.5% in aqueous solution), low cytotoxicity, and excellent photostability. Upon low power density excitation of continuous laser (wavelength 532 nm, 8.5 mW/cm^{-2}), upconversion luminescence imaging in cells and mice were demonstrated. The bioimaging results showed excellent signal-to-noise ratio (>25) using the UCNPs as the luminescence probe.

By loading different annihilator molecules into the silica nanoparticle, Kwon *et al*. prepared dual color TTA-based UCNPs for targeting and imaging tumors in mice (Fig. 13).[161] In these dual color UCNPs, PdTBP was employed as the sensitizer, and perylene (λ_{em} = 470 nm) and 9,10-bis(phenylethynyl)anthracene (DPEA) (λ_{em} = 505 nm) as the annihilator for preparing blue emission SNC-B, and green emission SNC-G, respectively. Amino surface functionalized SNC nanoparticles enable bioconjugation with cancer cell targeting molecules, such as anti-MUC1 antibody and TCP1

peptide. The upconversion luminescence imaging of breast cancer and colon cancer cells and tumor embedded mice was also demonstrated.

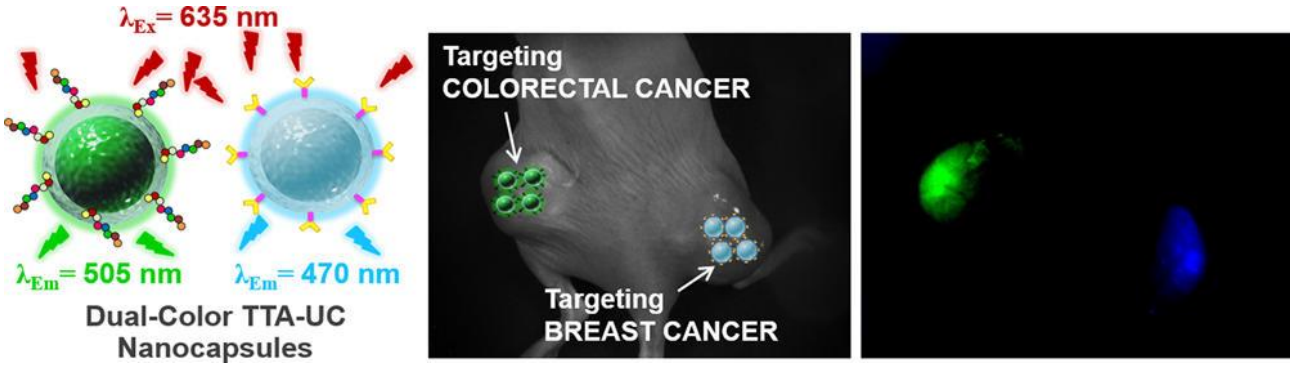

Fig. 13. Dual color TTA-UCNPs for cancer bioimaging in live mice. Reprinted with permission from ref.161. Copyright 2016 American Chemical Society.

Recently, silica coated upconversion liposome has been reported by Askes and colleagues.[142] In this work, the sensitizer and annihilator molecules (PdTPDBP-perylene/TBP pair) were firstly loaded into the liposome nanoencapulator, followed by the silica coating with three different methods. In solution and live A549 cells, no protection from oxygen quenching for silica coating was observed. However, clear blue upconversion luminescence was observed after heat-drying the nanoparticles in the presence of excess (organo)silica precursor in the air, suggesting that the thin silica layer cannot protect the upconversion luminescence from oxygen quenching in biological conditions.

6. Concluding remarks

This review has summarized recent developments of UCNPs and their biomedical applications, covering the mechanisms of Ln-doped, dye-sensitized, and TTA-based UCNPs, their preparation, surface modification and biomedical applications. It is clear that Ln-doped, dye-sensitized, and TTA-based UCNPs show great promise in biomedical applications owing to their unique photophysical properties (Table 1). Their capacity of converting low energy photons to high energy luminescent ones

allows NIR to be delivered into the deep biological tissues for light-based photobiological and photochemical processes. Despite the advancements of UCNPs in these aspects, the development of UCNPs for biomedical applications remains great challenges in future researches.

For Ln-doped UCNPs, biomedical applications are generally limited by their low upconversion efficiency, which can be attributed to the low absorption cross section of sensitisers (Ln^{3+}) (Table 1). Although considerable efforts have been devoted to increasing upconversion luminescence by exploring core-shell nanostructure and Ln-doping concentration, these luminescent UCNPs do improve the sensitivity for biosensing, bioimaging, and photo-initiated biological and chemical reactions, while high efficiency is still required. Furthermore, efficient upconversion is realised only upon the excitation with 980 nm and 808 nm laser, which have seriously hampered their practical applications in biomedical applications. Considering the applications of Ln-dopant UCNPs in biological species, systematic and comprehensive toxicology studies of these nanoparticles are still demanding for future pre-clinical and clinical applications. In addition, the surface of the prepared nanoparticles is generally stabilized with hydrophobic ligands, which are inappropriate for the applications in the biological conditions. Therefore, surface modification of Ln-UCNPs has been actively investigated in recent years, and several methods for surface modification have been successfully demonstrated. Even so, surface modification and bioconjugation of long-term stable and biocompatible Ln-UCNPs remains a challenge and more research is needed in future.

Currently, the low conversion efficiency and narrow-band near infrared absorption of Ln-doped UCNPs can also be overcome by incorporating single or multiple dye sensitisers, and a few of dye sensitizing organic-inorganic systems have been developed. However, the research efforts on this upconversion process have been mainly focused on the discovery of new organic dyes as the antenna, whereby the excitation light source can be extended, but biomedical applications of these emerging upconversion nanomaterials have been less investigated, limiting their usage in bioimaging and photodynamic therapy. Since most of the dye-sensitized upconversion is achieved in organic solvents, such as DMF, chloroform, the applications in aqueous solutions are thus very much challenging. The difficulty can be attributed to a few issues for dye-sensitized UCNPs in aqueous solutions, including (i)

detachment of dyes from organic-inorganic nanocomposites; (ii) rapid photo-bleaching of dyes; and (iii) quenching of upconversion luminescence. These issues cause low energy transfers from dye to Ln^{3+} sensitizer, which have to be overcome in the future biomedical applications.

Compared to Ln-doped UCNPs, TTA-based UCNPs have relatively higher luminescence efficiency (upconversion quantum yields of 17.4% was obtained at the excitation power density 0.5 W/cm^2). However, current investigations mainly focus on the design and synthesis of sensitiser and annihilator molecules, so it is necessary to develop water-soluble and oxygen-tolerable TTA-UCNP systems for biological applications. Taking advantages of TTA-based UCNPs, the future research should include their biosensing, bioimaging, cancer diagnosis and phototherapy, and photo-triggered drug delivery in aqueous solutions. Here, a few key factors must be considered to engineer TTA-based UCNPs for biomedical applications. Firstly, the novel matrix for developing oxygen-resistant TTA-based UCNPs is demanded since the TTA upconversion is oxygen sensitive. Secondly, current TTA-based UCNPs show higher upconversion efficiency, while the excitation and emission wavelengths mainly locate in the UV-visible range, which limits their biomedical applications due to the shallow tissue penetration. Therefore, development of sensitizers with intense absorption in the NIR range and annihilator molecules with emission in red and NIR range is desirable. Thirdly, the photostability of both sensitizer and annihilator molecules are relatively low under laser irradiation, so development of photostable TTA-based UCNPs is necessary. Finally, it seems that the toxicity of TTA-based UCNPs is normally lower than Ln-doped UCNPs, but the toxicity for both sensitizer and annihilator needs to be well evaluated since some heavy metal ions may be released and captured by live organisms after degradation in the body.

Table 1. Photophysical properties and biomedical applications of classic Ln-doped upconversion luminescence, dye-sensitized upconversion luminescence and TTA-upconversion luminescence.

Upconversion	**Excitation**	**Sensitisers**	**Absorption cross section (cm^2)**	**Laser power (W/cm^2)**	**Emission**	**ϕ_{UCL}**	**Biomedical applications**	**Reference**
Classical Ln-UCL	980 nm, 808 nm	Ln^{3+} (*e. g.* Yb^{3+} and Nd^{3+})	~ 10^{-20}	> 0.1	UV-NIR	~ 3% (ex 980 nm, 20 W/cm^2) 0.18 % (ex 800 nm, 31 W/cm^2)	Biosensing, bioimaging, theranostics	31, 120, 127, 162, 163
Dye-sensitized UCL	Vis-NIR	Organic dyes	> 10^{-17}	~0.016-10	UV-NIR	~ 5% (ex 800 nm, 2 W/cm^2)	Bioimaging PDT	42, 43, 144, 145
TTA-UCL	Vis-NIR	Organic dyes	> 10^{-17}	< 0.1	UV-Vis	17.4% (ex 532 nm, 0.5 W/cm^2)	Bioimaging	30, 153, 154, 161, 164

Acknowledgments

The authors gratefully acknowledge the financial support from Australian Research Council (DE170100092, DP170104643), National Health and Medical Research Council (APP1125794), and Advance Queensland Fellowship.

References

1. J. Yao, M. Yang and Y. Duan, *Chem. Rev.*, 2014, **114**, 6130-6178.
2. J. Weber, P. C. Beard and S. E. Bohndiek, *Nat. Methods*, 2016, **13**, 639-650.
3. L. V. Wang and J. Yao, *Nat. Methods*, 2016, **13**, 627-638.
4. L. Ling, Z. Run, G. Yi, Z. Cheng, Z. Wei, X. Zhiping and K. W. Andrew, *Nanotechnology*, 2016, **27**, 485702.
5. L. Li, Y. Q. Wu, K. K. Sun, R. Zhang, L. Fan, K. K. Liang and L. B. Mao, *Mater. Lett.*, 2016, **162**, 207-210.
6. S. Kunjachan, J. Ehling, G. Storm, F. Kiessling and T. Lammers, *Chem. Rev.*, 2015, **115**, 10907-10937.
7. Y. Zhang, Y. Guo, Y. Xianyu, W. Chen, Y. Zhao and X. Jiang, *Adv. Mater.*, 2013, **25**, 3802-3819.
8. J. Yuan and G. Wang, *Trends Anal. Chem.*, 2006, **25**, 490-500.
9. S. E. Webber, *Macromol. Symp.*, 1999, **143**, 359-370.
10. H. Tan, B. Liu and Y. Chen, *ACS Nano*, 2012, **6**, 10505-10511.
11. F. Pinaud, X. Michalet, L. A. Bentolila, J. M. Tsay, S. Doose, J. J. Li, G. Iyer and S. Weiss, *Biomaterials*, 2006, **27**, 1679-1687.
12. X. Liang, H. Wang, Y. Zhu, R. Zhang, V. C. Cogger, X. Liu, Z. P. Xu, J. E. Grice and M. S. Roberts, *ACS Nano*, 2016, **10**, 387-395.
13. X. Yuan, Z. Luo, Y. Yu, Q. Yao and J. Xie, *Chem. Asian J.*, 2013, **8**, 858-871.
14. S. W. Bae, W. Tan and J.-I. Hong, *Chem. Commun.*, 2012, **48**, 2270-2282.
15. J. Zhou, Q. Liu, W. Feng, Y. Sun and F. Li, *Chem. Rev.*, 2015, **115**, 395-465.
16. J. Zhang, Y. Yang, C. Mi, Y. Liu, F. Yu, X. Li and Y. Mai, *Dalton Trans.*, 2015, **44**, 1093-1101.
17. Q. Liu, W. Feng, T. Yang, T. Yi and F. Li, *Nat. Protoc.*, 2013, **8**, 2033-2044.
18. L. Cheng, C. Wang, L. Feng, K. Yang and Z. Liu, *Chem. Rev.*, 2014, **114**, 10869-10939.
19. N. Mitter, E. A. Worrall, K. E. Robinson, P. Li, R. G. Jain, C. Taochy, S. J. Fletcher, B. J. Carroll, G. Q. Lu and Z. P. Xu, *Nat. Plants*, 2017, **3**, 16207.
20. L. Li, Z. Gu, W. Gu, J. Liu and Z. P. Xu, *J. Colloid Interface Sci.*, 2016, **470**, 47-55.
21. K. Sun, L. Li, X. Yu, L. Liu, Q. Meng, F. Wang and R. Zhang, *J. Colloid Interface Sci.*, 2017, **486**, 128-135.
22. L. Li, W. Gu, J. Liu, S. Yan and Z. P. Xu, *Nano Res.*, 2015, **8**, 682-694.
23. V. Muhr, S. Wilhelm, T. Hirsch and O. S. Wolfbeis, *Acc. Chem. Res.*, 2014, **47**, 3481-3493.
24. X. Zhu, Q. Su, W. Feng and F. Li, *Chem. Soc. Rev.*, 2017, **46**, 1025-1039.
25. E. M. Chan, G. Han, J. D. Goldberg, D. J. Gargas, A. D. Ostrowski, P. J. Schuck, B. E. Cohen and D. J. Milliron, *Nano Lett.*, 2012, **12**, 3839-3845.
26. L. Liang, A. Care, R. Zhang, Y. Lu, N. H. Packer, A. Sunna, Y. Qian and A. V. Zvyagin, *ACS Appl. Mater. Interfaces*, 2016, **8**, 11945-11953.
27. L. Liang, Y. Lu, R. Zhang, A. Care, T. A. Ortega, S. M. Deyev, Y. Qian and A. V. Zvyagin, *Acta Biomater.*, 2017, **51**, 461-470.
28. J. Zhao, S. Ji and H. Guo, *RSC Adv.*, 2011, **1**, 937-950.
29. S. Ji, W. Wu, W. Wu, H. Guo and J. Zhao, *Angew. Chem. Int. Ed.*, 2011, **50**, 1626-1629.
30. C. Ye, L. Zhou, X. Wang and Z. Liang, *Phys. Chem. Chem. Phys.*, 2016, **18**, 10818-10835.
31. H. Dong, L.-D. Sun and C.-H. Yan, *Chem. Soc. Rev.*, 2015, **44**, 1608-1634.
32. F. Zhang, in *Photon Upconversion Nanomaterials*, Springer Berlin Heidelberg, Berlin, Heidelberg, 2015, DOI: 10.1007/978-3-662-45597-5_1, pp. 1-20.
33. X. Li, F. Zhang and D. Zhao, *Chem. Soc. Rev.*, 2015, **44**, 1346-1378.
34. Q. Su, W. Feng, D. Yang and F. Li, *Acc. Chem. Res.*, 2017, **50**, 32-40.

35. F. Wang and X. Liu, *Chem. Soc. Rev.*, 2009, **38**, 976-989.
36. F. Wang, R. Deng, J. Wang, Q. Wang, Y. Han, H. Zhu, X. Chen and X. Liu, *Nat. Mater.*, 2011, **10**, 968-973.
37. B. Zhou, B. Shi, D. Jin and X. Liu, *Nat. Nanotechnol.*, 2015, **10**, 924-936.
38. G. Chen and G. Han, *Theranostics*, 2013, **3**, 289.
39. Y. Lu, J. Zhao, R. Zhang, Y. Liu, D. Liu, E. M. Goldys, X. Yang, P. Xi, A. Sunna, J. Lu, Y. Shi, R. C. Leif, Y. Huo, J. Shen, J. A. Piper, J. P. Robinson and D. Jin, *Nat. Photonics*, 2014, **8**, 32-36.
40. S. Wu, G. Han, D. J. Milliron, S. Aloni, V. Altoe, D. V. Talapin, B. E. Cohen and P. J. Schuck, *Proc. Natl. Acad. Sci.*, 2009, **106**, 10917-10921.
41. X. Huang, *J. Alloys Compd.*, 2017, **690**, 356-359.
42. W. Zou, C. Visser, J. A. Maduro, M. S. Pshenichnikov and J. C. Hummelen, *Nat. Photonics*, 2012, **6**, 560-564.
43. G. Chen, J. Damasco, H. Qiu, W. Shao, T. Y. Ohulchanskyy, R. R. Valiev, X. Wu, G. Han, Y. Wang and C. Yang, *Nano Lett.*, 2015, **15**, 7400-7407.
44. C. D. LaBoda and C. L. Dwyer, *Adv. Funct. Mater.*, 2016, **26**, 2866-2874.
45. X. Xie and X. Liu, *Nat. Materials*, 2012, **11**, 842.
46. X. Wang, R. R. Valiev, T. Y. Ohulchanskyy, H. Ågren, C. Yang and G. Chen, *Chem. Soc. Rev.*, 2017, **46**, 4150-4167.
47. J. Zhao, S. Ji, W. Wu, W. Wu, H. Guo, J. Sun, H. Sun, Y. Liu, Q. Li and L. Huang, *RSC Adv.*, 2012, **2**, 1712-1728.
48. J. Zhao, W. Wu, J. Sun and S. Guo, *Chem. Soc. Rev.*, 2013, **42**, 5323-5351.
49. T. N. Singh-Rachford and F. N. Castellano, *Coord. Chem. Rev.*, 2010, **254**, 2560-2573.
50. Y. C. Simon and C. Weder, *J. Mater. Chem.*, 2012, **22**, 20817-20830.
51. L. Cao, R. Zhang, W. Zhang, Z. Du, C. Liu, Z. Ye, B. Song and J. Yuan, *Biomaterials*, 2015, **68**, 21-31.
52. W. Zhang, F. Zhang, Y.-L. Wang, B. Song, R. Zhang and J. Yuan, *Inorg. Chem.*, 2017, **56**, 1309-1318.
53. S. Ji, H. Guo, W. Wu, W. Wu and J. Zhao, *Angew. Chem. Int. Ed.*, 2011, **50**, 8283-8286.
54. F. Zhang, X. Liang, W. Zhang, Y.-L. Wang, H. Wang, Y. H. Mohammed, B. Song, R. Zhang and J. Yuan, *Biosens. Bioelectron.*, 2017, **87**, 1005-1011.
55. R. Wang, D. Liu, R. Zhang, L. Deng and J. Li, *J. Mater. Chem.*, 2012, **22**, 1411-1417.
56. R. Wang, D. Liu, H. Ren, T. Zhang, X. Wang and J. Li, *J. Mater. Chem.*, 2011, **21**, 15494-15500.
57. W. Wu, J. Zhao, H. Guo, J. Sun, S. Ji and Z. Wang, *Chem. Eur. J.*, 2012, **18**, 1961-1968.
58. H. Guo, Q. Li, L. Ma and J. Zhao, *J. Mater. Chem.*, 2012, **22**, 15757-15768.
59. Y.-W. Zhang, X. Sun, R. Si, L.-P. You and C.-H. Yan, *J. Am. Chem. Soc.*, 2005, **127**, 3260-3261.
60. Z. Li and Y. Zhang, *Nanotechnology*, 2008, **19**, 5.
61. F. Wang, Y. Han, C. S. Lim, Y. Lu, J. Wang, J. Xu, H. Chen, C. Zhang, M. Hong and X. Liu, *Nature*, 2010, **463**, 1061-1065.
62. A. D. Ostrowski, E. M. Chan, D. J. Gargas, E. M. Katz, G. Han, P. J. Schuck, D. J. Milliron and B. E. Cohen, *ACS nano*, 2012, **6**, 2686-2692.
63. Q. Liu, Y. Sun, T. Yang, W. Feng, C. Li and F. Li, *J. Am. Chem. Soc.*, 2011, **133**, 17122-17125.
64. X. Wang, J. Zhuang, Q. Peng and Y. Li, *Nature*, 2005, **437**, 121-124.
65. F. Wang, D. K. Chatterjee, Z. Li, Y. Zhang, X. Fan and M. Wang, *Nanotechnology*, 2006, **17**, 5786.
66. F. Zhang, Y. Wan, T. Yu, F. Zhang, Y. Shi, S. Xie, Y. Li, L. Xu, B. Tu and D. Zhao, *Angew. Chem. Int. Ed.*, 2007, **46**, 7976-7979.
67. G.-S. Yi and G.-M. Chow, *Chem. Mater.*, 2007, **19**, 341-343.
68. F. Vetrone, R. Naccache, V. Mahalingam, C. G. Morgan and J. A. Capobianco, *Adv. Funct. Mater.*, 2009, **19**, 2924-2929.
69. X. Liu, X. Kong, Y. Zhang, L. Tu, Y. Wang, Q. Zeng, C. Li, Z. Shi and H. Zhang, *Chem. Commun.*, 2011, **47**, 11957-11959.
70. Z. Chen, H. Chen, H. Hu, M. Yu, F. Li, Q. Zhang, Z. Zhou, T. Yi and C. Huang, *J. Am. Chem. Soc.*, 2008, **130**, 3023-3029.
71. H. P. Zhou, C. H. Xu, W. Sun and C. H. Yan, *Adv. Funct. Mater.*, 2009, **19**, 3892-3900.
72. R. Naccache, F. Vetrone, V. Mahalingam, L. A. Cuccia and J. A. Capobianco, *Chem. Mater.*, 2009, **21**, 717-723.
73. M. Wang, J.-L. Liu, Y.-X. Zhang, W. Hou, X.-L. Wu and S.-K. Xu, *Mater. Lett.*, 2009, **63**, 325-327.
74. N. Bogdan, F. Vetrone, G. A. Ozin and J. A. Capobianco, *Nano Lett.*, 2011, **11**, 835-840.
75. W. Kong, T. Sun, B. Chen, X. Chen, F. Ai, X. Zhu, M. Li, W. Zhang, G. Zhu and F. Wang, *Inorg. Chem.*, 2017.
76. N. Bogdan, E. M. Rodríguez, F. Sanz-Rodríguez, M. C. I. de la Cruz, Á. Juarranz, D. Jaque, J. G. Solé and J. A. Capobianco, *Nanoscale*, 2012, **4**, 3647-3650.
77. G. Jiang, J. Pichaandi, N. J. Johnson, R. D. Burke and F. C. van Veggel, *Langmuir*, 2012, **28**, 3239-3247.

78. L. Cheng, K. Yang, M. Shao, S.-T. Lee and Z. Liu, *J. Phys. Chem. C*, 2011, **115**, 2686-2692.
79. L. Cheng, K. Yang, S. Zhang, M. Shao, S. Lee and Z. Liu, *Nano Res.,* 2010, **3**, 722-732.
80. S. J. Budijono, J. Shan, N. Yao, Y. Miura, T. Hoye, R. H. Austin, Y. Ju and R. K. Prud'homme, *Chem. Mater.*, 2009, **22**, 311-318.
81. S. Liang, X. Zhang, Z. Wu, Y. Liu, H. Zhang, H. Sun, H. Sun and B. Yang, *CrystEngComm*, 2012, **14**, 3484-3489.
82. L. L. Li, R. Zhang, L. Yin, K. Zheng, W. Qin, P. R. Selvin and Y. Lu, *Angew. Chem. Int. Ed.*, 2012, **51**, 6121-6125.
83. J. Shan, S. J. Budijono, G. Hu, N. Yao, Y. Kang, Y. Ju and R. K. Prud'homme, *Adv. Funct. Mater.*, 2011, **21**, 2488-2495.
84. S. Huang, M. Bai and L. Wang, *Sci. Rep.*, 2013, **3**.
85. Y. Guan, H. Lu, W. Li, Y. Zheng, Z. Jiang, J. Zou and H. Gao, *ACS Appl. Mater. Interfaces*, 2017, **9**, 26731-26739.
86. C. Yao, P. Wang, L. Zhou, R. Wang, X. Li, D. Zhao and F. Zhang, *Anal. Chem.*, 2014, **86**, 9749-9757.
87. Z. Wu, C. Guo, S. Liang, H. Zhang, L. Wang, H. Sun and B. Yang, *J. Mater. Chem.*, 2012, **22**, 18596-18602.
88. T. Zhang, J. Ge, Y. Hu and Y. Yin, *Nano Lett.*, 2007, **7**, 3203-3207.
89. Q. Zhang, K. Song, J. Zhao, X. Kong, Y. Sun, X. Liu, Y. Zhang, Q. Zeng and H. Zhang, *J. Colloid Interface Sci.*, 2009, **336**, 171-175.
90. F. Meiser, C. Cortez and F. Caruso, *Angew. Chem. Inter. Ed.*, 2004, **43**, 5954-5957.
91. R. Kumar, M. Nyk, T. Y. Ohulchanskyy, C. A. Flask and P. N. Prasad, *Adv. Funct. Mater.*, 2009, **19**, 853-859.
92. G. S. Yi and G. M. Chow, *Adv. Funct. Mater.*, 2006, **16**, 2324-2329.
93. L. Xiong, B. Shen, D. Behera, S. S. Gambhir, F. T. Chin and J. Rao, *Nanoscale*, 2013, **5**, 3253-3256.
94. R. Qiao, C. Liu, M. Liu, H. Hu, C. Liu, Y. Hou, K. Wu, Y. Lin, J. Liang and M. Gao, *ACS Nano*, 2015, **9**, 2120-2129.
95. R. Liu, D. Tu, Y. Liu, H. Zhu, R. Li, W. Zheng, E. Ma and X. Chen, *Nanoscale*, 2012, **4**, 4485-4491.
96. J. Lu, Y. Chen, D. Liu, W. Ren, Y. Lu, Y. Shi, J. Piper, I. Paulsen and D. Jin, *Anal. Chem.*, 2015, **87**, 10406-10413.
97. N. Bogdan, F. Vetrone, R. Roy and J. A. Capobianco, *J. Mater. Chem.*, 2010, **20**, 7543-7550.
98. G. Yi, Y. Peng and Z. Gao, *Chem. Mater.*, 2011, **23**, 2729-2734.
99. L. Xia, X. Kong, X. Liu, L. Tu, Y. Zhang, Y. Chang, K. Liu, D. Shen, H. Zhao and H. Zhang, *Biomaterials*, 2014, **35**, 4146-4156.
100. Y. Li, J. Tang, L. He, Y. Liu, Y. Liu, C. Chen and Z. Tang, *Adv. Mater.*, 2015, **27**, 4075-4080.
101. A. E. Guller, A. N. Generalova, E. V. Petersen, A. V. Nechaev, I. A. Trusova, N. N. Landyshev, A. Nadort, E. A. Grebenik, S. M. Deyev and A. B. Shekhter, *Nano Res.*, 2015, **8**, 1546-1562.
102. A. Dong, X. Ye, J. Chen, Y. Kang, T. Gordon, J. M. Kikkawa and C. B. Murray, *J. Am. Chem. Soc.*, 2010, **133**, 998-1006.
103. J.-C. Boyer, M.-P. Manseau, J. I. Murray and F. C. van Veggel, *Langmuir*, 2009, **26**, 1157-1164.
104. I. Recalde, N. Estebanez, L. Francés-Soriano, M. Liras, M. González-Béjar and J. Pérez-Prieto, *Nanoscale*, 2016, **8**, 7588-7594.
105. M. Lin, Y. Gao, T. J. Diefenbach, J. K. Shen, F. J. Hornicek, Y. I. Park, F. Xu, T. J. Lu, M. Amiji and Z. Duan, *ACS Appl. Mater. Interfaces*, 2017, **9**, 7941.
106. L. Wang, R. Yan, Z. Huo, L. Wang, J. Zeng, J. Bao, X. Wang, Q. Peng and Y. Li, *Angew. Chem. Int. Ed.*, 2005, **44**, 6054-6057.
107. H. Xing, W. Bu, S. Zhang, X. Zheng, M. Li, F. Chen, Q. He, L. Zhou, W. Peng and Y. Hua, *Biomaterials*, 2012, **33**, 1079-1089.
108. Z. Li and Y. Zhang, *Angew. Chem. Int. Ed.* 2006, **45**, 7732-7735.
109. J.-N. Liu, W.-B. Bu and J.-L. Shi, *Acc. Chem. Res.*, 2015, **48**, 1797-1805.
110. H. S. Qian, H. C. Guo, P. C. L. Ho, R. Mahendran and Y. Zhang, *Small*, 2009, **5**, 2285-2290.
111. J. Liu, J. Bu, W. Bu, S. Zhang, L. Pan, W. Fan, F. Chen, L. Zhou, W. Peng and K. Zhao, *Angew. Chem. Int. Ed.*, 2014, **53**, 4551-4555.
112. M. Darbandi and T. Nann, *Chem. Commun.*, 2006, 776-778.
113. M. Wang, C. Mi, Y. Zhang, J. Liu, F. Li, C. Mao and S. Xu, *J. Phys. Chem. C*, 2009, **113**, 19021-19027.
114. N. M. Idris, M. K. Gnanasammandhan, J. Zhang, P. C. Ho, R. Mahendran and Y. Zhang, *Nat. Med.*, 2012, **18**, 1580-1585.
115. S. Xu, S. Huang, Q. He and L. Wang, *Trends Anal. Chem.*, 2015, **66**, 72-79.
116. S. Gai, C. Li, P. Yang and J. Lin, *Chem. Rev.*, 2014, **114**, 2343-2389.
117. J. Zhao, D. Jin, E. P. Schartner, Y. Lu, Y. Liu, A. V. Zvyagin, L. Zhang, J. M. Dawes, P. Xi, J. A. Piper, E. M. Goldys and T. M. Monro, *Nat. Nanotechnol.* 2013, **8**, 729.

118. Y. Liu, Y. Lu, X. Yang, X. Zheng, S. Wen, F. Wang, X. Vidal, J. Zhao, D. Liu, Z. Zhou, C. Ma, J. Zhou, J. A. Piper, P. Xi and D. Jin, *Nature*, 2017, **543**, 229-233.
119. L. Xiong, Z. Chen, Q. Tian, T. Cao, C. Xu and F. Li, *Anal. Chem.*, 2009, **81**, 8687-8694.
120. G. Chen, J. Shen, T. Y. Ohulchanskyy, N. J. Patel, A. Kutikov, Z. Li, J. Song, R. K. Pandey, H. Ågren and P. N. Prasad, *ACS Nano*, 2012, **6**, 8280.
121. Y. I. Park, H. M. Kim, J. H. Kim, K. C. Moon, B. Yoo, K. T. Lee, N. Lee, Y. Choi, W. Park and D. Ling, *Adv. Mater.*, 2012, **24**, 5755-5761.
122. X. Zhu, J. Zhou, M. Chen, M. Shi, W. Feng and F. Li, *Biomaterials*, 2012, **33**, 4618-4627.
123. Q. Liu, Y. Sun, C. Li, J. Zhou, C. Li, T. Yang, X. Zhang, T. Yi, D. Wu and F. Li, *ACS Nano*, 2011, **5**, 3146-3157.
124. Q. Su, W. Feng, D. Yang and F. Li, *Acc. Chem. Res.,* 2017, **50**, 32-40
125. J. Chen and J. X. Zhao, *Sensors*, 2012, **12**, 2414-2435.
126. V. Muhr, C. Würth, M. Kraft, M. Buchner, A. J. Baeumner, U. Resch-Genger and T. Hirsch, *Anal. Chem.*, 2017, **89**, 4868-4874.
127. J. Liu, Y. Liu, Q. Liu, C. Li, L. Sun and F. Li, *J. Am. Chem. Soc.*, 2011, **133**, 15276-15279.
128. L. Yao, J. Zhou, J. Liu, W. Feng and F. Li, *Adv. Funct. Mater.*, 2012, **22**, 2667-2672.
129. P. Zhang, S. Rogelj, K. Nguyen and D. Wheeler, *J. Am. Chem. Soc.*, 2006, **128**, 12410-12411.
130. M. Wang, W. Hou, C.-C. Mi, W.-X. Wang, Z.-R. Xu, H.-H. Teng, C.-B. Mao and S.-K. Xu, *Anal. Chem.*, 2009, **81**, 8783-8789.
131. M. Kumar and P. Zhang, *Langmuir*, 2009, **25**, 6024-6027.
132. N. M. Idris, M. K. G. Jayakumar, A. Bansal and Y. Zhang, *Chem. Soc. Rev.*, 2015, **44**, 1449-1478.
133. D. Yang, Z. Hou, Z. Cheng, C. Li and J. Lin, *Chem. Soc. Rev.*, 2015, **44**, 1416-1448.
134. J. Liu, W. Bu, L. Pan and J. Shi, *Angew. Chem. Int. Ed.*, 2013, **52**, 4375-4379.
135. A. Punjabi, X. Wu, A. Tokatli-Apollon, M. El-Rifai, H. Lee, Y. Zhang, C. Wang, Z. Liu, E. M. Chan and C. Duan, *ACS Nano*, 2014, **8**, 10621-10630.
136. C. Wang, L. Cheng and Z. Liu, *Theranostics*, 2013, **3**, 317-330.
137. Q. Shao, X. Li, P. Hua, G. Zhang, Y. Dong and J. Jiang, *J. Colloid Interface Sci.*, 2017, **486**, 121-127 %@ 0021-9797.
138. X. Wu, H. Lee, O. Bilsel, Y. Zhang, Z. Li, T. Chen, Y. Liu, C. Duan, J. Shen and A. Punjabi, *Nanoscale*, 2015, **7**, 18424-18428.
139. W. Shao, G. Chen, A. Kuzmin, H. L. Kutscher, A. Pliss, T. Y. Ohulchanskyy and P. N. Prasad, *J. Am. Chem. Soc.*, 2016, **138**, 16192-16195.
140. W. Wei, G. Chen, A. Baev, G. S. He, W. Shao, J. Damasco and P. N. Prasad, *J. Am. Chem. Soc.*, 2016, **138**, 15130-15133.
141. G. Chen, T. Y. Ohulchanskyy, R. Kumar, H. Ågren and P. N. Prasad, *ACS Nano*, 2010, **4**, 3163-3168.
142. S. H. C. Askes, V. C. Leeuwenburgh, W. Pomp, H. Arjmandi-Tash, S. Tanase, T. Schmidt and S. Bonnet, *ACS Biomater. Sci. Eng.*, 2017, **3**, 322-334.
143. X. Zou, M. Xu, W. Yuan, Q. Wang, Y. Shi, W. Feng and F. Li, *Chem. Commun.*, 2016, **52**, 13389-13392.
144. X. Wu, Y. Zhang, K. Takle, O. Bilsel, Z. Li, H. Lee, Z. Zhang, D. Li, W. Fan and C. Duan, *ACS Nano*, 2016, **10**, 1060-1066.
145. J. Xu, P. Yang, M. Sun, H. Bi, B. Liu, D. Yang, S. Gai, F. He and J. Lin, *ACS Nano*, 2017, **11**, 4133-4144.
146. A. Turshatov, D. Busko, N. Kiseleva, S. L. Grage, I. A. Howard and B. S. Richards, *ACS Appl. Mater. Interfaces*, 2017, **9**, 8280-8286.
147. S. H. C. Askes, W. Pomp, S. L. Hopkins, A. Kros, S. Wu, T. Schmidt and S. Bonnet, *Small*, 2016, **12**, 5579-5590.
148. Y. C. Simon, S. Bai, M. K. Sing, H. Dietsch, M. Achermann and C. Weder, *Macromol, Rapid Commun,*, 2012, **33**, 498-502.
149. C. Wohnhaas, A. Turshatov, V. Mailänder, S. Lorenz, S. Baluschev, T. Miteva and K. Landfester, *Macromol, Biosci,*, 2011, **11**, 772-778.
150. C. Wohnhaas, V. Mailänder, M. Dröge, M. A. Filatov, D. Busko, Y. Avlasevich, S. Baluschev, T. Miteva, K. Landfester and A. Turshatov, *Macromolecular Bioscience*, 2013, **13**, 1422-1430.
151. C. Wohnhaas, K. Friedemann, D. Busko, K. Landfester, S. Baluschev, D. Crespy and A. Turshatov, *ACS Macro Lett.*, 2013, **2**, 446-450.
152. K. Katta, D. Busko, Y. Avlasevich, R. Muñoz-Espí, S. Baluschev and K. Landfester, *Macromol. Rapid Commun.*, 2015, **36**, 1084-1088.
153. W. Wang, Q. Liu, C. Zhan, A. Barhoumi, T. Yang, R. G. Wylie, P. A. Armstrong and D. S. Kohane, *Nano Lett.*, 2015, **15**, 6332-6338.
154. Q. Liu, B. Yin, T. Yang, Y. Yang, Z. Shen, P. Yao and F. Li, *J. Am. Chem. Soc.*, 2013, **135**, 5029-5037.
155. B. Tian, Q. Wang, Q. Su, W. Feng and F. Li, *Biomaterials*, 2017, **112**, 10-19.

156. T. Andrey, B. Dmitry, B. Stanislav, M. Tzenka and L. Katharina, *New J. Phys.*, 2011, **13**, 083035.
157. X. Cao, L. Bao, Y. Zhou, J. Zhang and R. Ding, *Nano LIFE*, 2016, **06**, 1642010.
158. O. S. Kwon, J.-H. Kim, J. K. Cho and J.-H. Kim, *ACS Appl. Mater. Interfaces*, 2015, **7**, 318-325.
159. G. Massaro, P. L. Gentili, V. Ambrogi, M. Nocchetti, F. Marmottini, F. Ortica and L. Latterini, *Microporous Mesoporous Mater.*, 2017, **246**, 120-129.
160. Q. Liu, T. Yang, W. Feng and F. Li, *J. Am. Chem. Soc.*, 2012, **134**, 5390-5397.
161. O. S. Kwon, H. S. Song, J. Conde, H.-i. Kim, N. Artzi and J.-H. Kim, *ACS Nano*, 2016, **10**, 1512-1521.
162. J.-C. Boyer and F. C. J. M. van Veggel, *Nanoscale*, 2010, **2**, 1417-1419.
163. B. Liu, Y. Chen, C. Li, F. He, Z. Hou, S. Huang, H. Zhu, X. Chen and J. Lin, *Adv. Funct. Mater.*, 2015, **25**, 4717-4729.
164. Z.-Q. Liang, B. Sun, C.-Q. Ye, X.-M. Wang, X.-T. Tao, Q.-H. Wang, P. Ding, B. Wang and J.-J. Wang, *ChemPhysChem*, 2013, **14**, 3517-3522.

Table of Contents

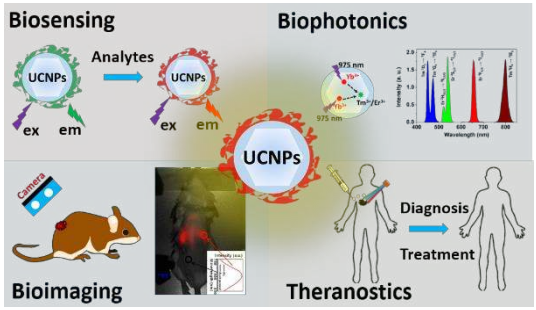

This review focuses on the biomedical applications of upconversion luminescence nanomaterials, including lanthanide-doped inorganic nanocrystals and TTA-based UCNPs.